THE UNIVERSITY OF TULSA

THE GRADUATE SCHOOL

INVESTIGATION OF THE EFFECTS OF COMPLETION GEOMETRIES UPON SINGLE PHASE LIQUID FLOW BEHAVIOR IN HORIZONTAL WELLS

By
Weipeng Jiang

A thesis submitted in partial fulfillment of

the requirements for the degree of Master's of Science

in the Discipline of Petroleum Engineering

The Graduate School

The University of Tulsa

1999

1. INTRODUCTION

Over the last decade, the use of horizontal wells has become a well-established practice for the recovery of oil and gas. It has become increasingly attractive for the production of thin-layered reservoirs, naturally fractured reservoirs, reservoirs with gas or water coning problems, offshore environments where various wells are drilled from a central platform, and also in enhanced oil recovery practices such as steam injection. Horizontal wells can also have many potential applications in the environmental industry.

Horizontal wells can improve the inflow performance of certain reservoirs, and can produce more oil with smaller pressure drawdowns compared to conventional vertical wells. However, the flow behavior in horizontal wells is highly complicated and is still the subject of extensive research in petroleum industry. Accurate modeling of pressure drop behavior in horizontal wells poses additional challenges to both reservoir engineers and production engineers.

The most commonly used assumptions in studying horizontal well production behavior are infinite conductivity and uniform influx (Fig. 1-1). Infinite conductivity assumes no pressure drop along a horizontal well, and uniform influx assumes that the influx from the reservoir is constant along a horizontal well. It has been argued in the literature that the infinite conductivity wellbore assumption is adequate for describing flow behavior in horizontal wells. Although this may be a good assumption in situations where the pressure drop along the horizontal section of the wellbore is negligible

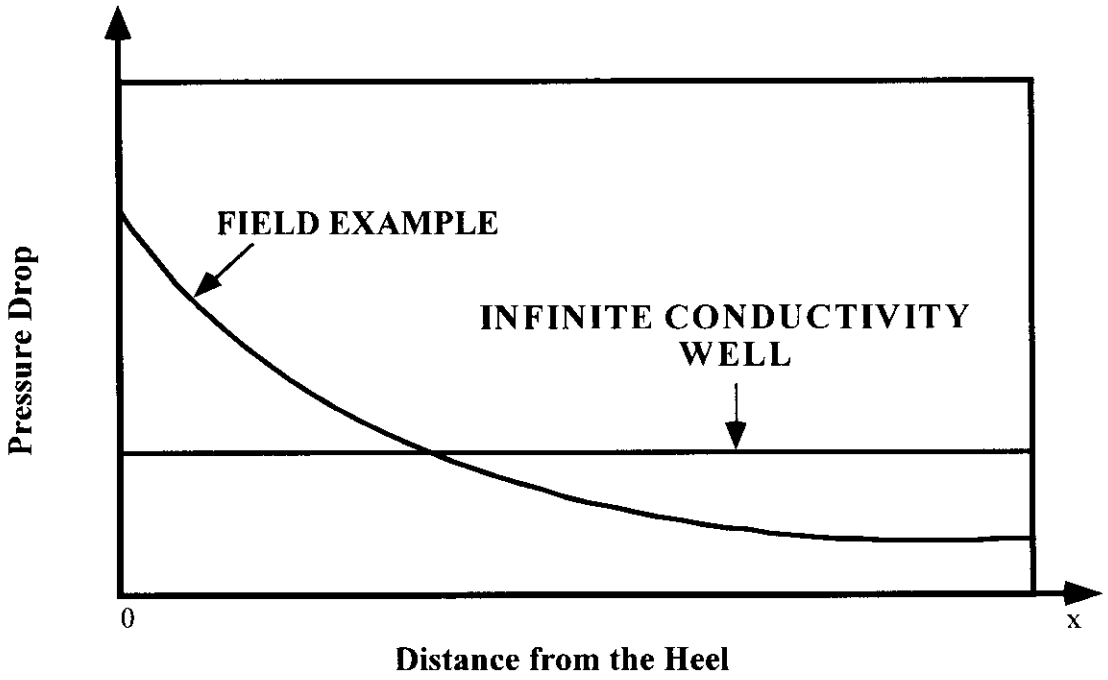

(a) Pressure Distribution Along a Horizontal Well

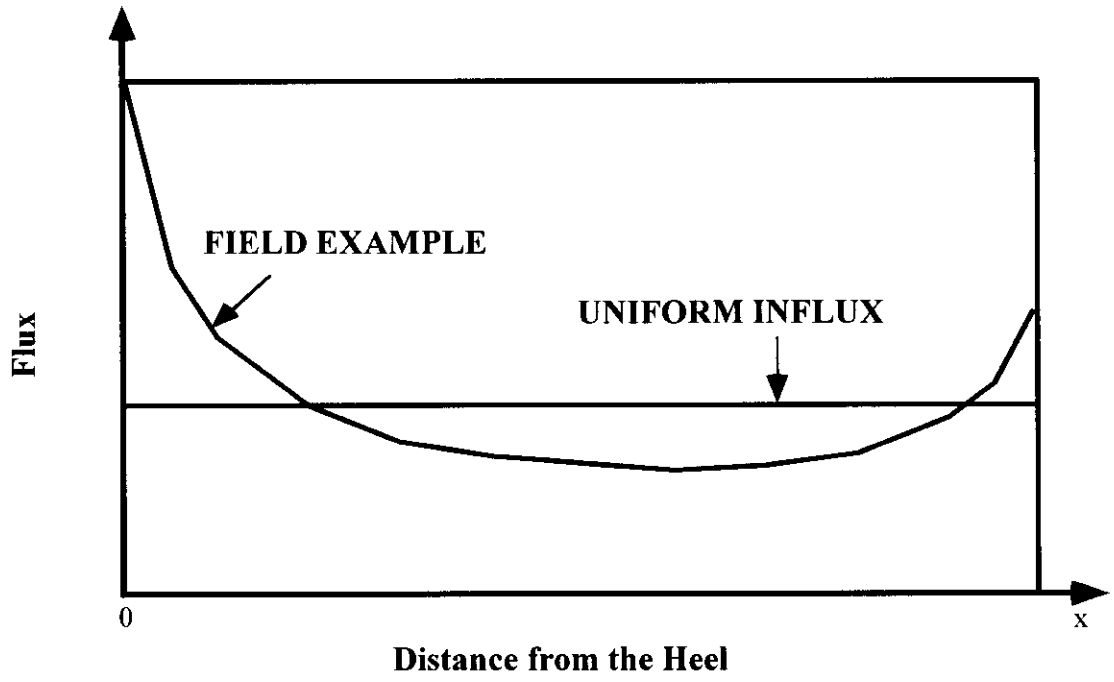

(b) Flux Distribution Along a Horizontal Well

Figure 1-1: Infinite Conductivity and Uniform Influx Assumptions and Comparisons with Field Examples

compared to that in the reservoir, it is also reasonable to expect the frictional and accelerational pressure losses to cause noticeable pressure drops in long horizontal wellbores. The flow behavior in a horizontal wellbore differs from flow in a regular pipe. Roughness of a horizontal well can be much higher than that of a regular pipe due to perforations and slots. Influxes along the wellbore, which cause momentum changes, can also change the pressure distribution. Therefore, the regular pipe friction factor correlations can not be used without modification to predict pressure drop in a horizontal well.

In a horizontal well, depending upon the completion method, fluid may enter the wellbore at various locations along the well length. The distance between perforations may not be sufficient to achieve a stabilized velocity profile, and this may lead to different pressure behaviors other than fully developed flow. Due to flow development, for example, the laminar flow regime can have as high as three to four times more pressure drop than for fully developed laminar flow situations. In the turbulent flow regime, the problem becomes more complicated, and therefore it is more difficult to predict the pressure distribution. The pressure distribution in a horizontal well can influence the well completion and well profile design, as well as having an impact on the production behavior of the well. Therefore, both the pressure drop vs. flow behavior along the well and the relationship between the pressure drop along the well and the influx from the reservoir need to be studied.

The objective of this experimental study is to investigate the flow behavior in perforated horizontal wells and horizontal wells completed with multiple slot liners. A

small scale TUFFP (Tulsa University Fluid Flow Projects) horizontal well test facility was modified to investigate the effect of completion geometries, such as the geometry of injection openings and the density and distribution of the injection openings, on the flow behavior in horizontal wells.

This study can be considered as a natural extension of those studies previously undertaken by Hong Yuan of TUFFP from 1994 to 1997. Yuan first experimentally investigated the flow behavior in a horizontal pipe with fluid injection from the pipe wall through a single injection point and obtained a lot of qualitative knowledge concerning the interactions between the main flow and the influx. Later Yuan conducted experiments investigating the flow behavior in multiple perforated horizontal wells and horizontal wells completed with multiple slot liners. By using the principles of mass and momentum conservation, general horizontal well friction factor expressions were developed for both the perforated horizontal wells and horizontal wells completed with slot liners (a total number of 7 test sections were included in her study).

In this study, six new test sections are designed and manufactured to investigate the flow behaviors in horizontal wells with multiple perforation completion. The perforation densities investigated are 5, 10 and 20 shots per foot and the perforation phasings investigated are 360^{o}, 180^{o} and 90^{o}. Four new test sections are designed and manufactured for horizontal wells completed with multiple slotted liners. The numbers of slots for those multiple slot cases are 18, 12 and 36 on a 4-ft. long test section. The slot phasings considered in this work are 360^{o}, 180^{o} and 90^{o}. Experimental data were acquired for flow rates, temperatures, and pressure drops under various Reynolds numbers and influx to main flow rate ratios. Based on the data acquired in this study and those data

obtained by Yuan, general apparent friction factor correlations were developed from the conservation of mass and momentum principles. The friction factor correlations can be used for various completion scenarios to get good estimations of the pressure drop behaviors in completed horizontal wells.

THE UNIVERSITY OF TULSA

THE GRADUATE SCHOOL

INVESTIGATION OF THE EFFECTS

OF COMPLETION GEOMETRIES

UPON SINGLE PHASE

LIQUID FLOW BEHAVIOR IN HORIZONTAL WELLS

By
Weipeng Jiang

A THESIS

APPROVED FOR THE DISCIPLINE OF

PETROLEUM ENGINEERING

By Thesis Committee

_____, Co-chairman

_____, Co-chairman

_____ _____

ABSTRACT

Jiang, Weipeng (Master of Science in Petroleum Engineering)

Investigation of the Effects of Completion Geometries upon Single Phase Liquid Flow Behavior in Horizontal Wells (75 pp. – Chapter VIII)

Co-directed by Dr. Cem Sarica and Dr. Mohan Kelkar

(130 words)

The petroleum fluid in horizontal wells can have very complicated flow behaviors, in part due to interaction between the main flow and the influxes along the well bore, and also due to completion geometries.

An existing small-scale test facility at TUFFP (Tulsa University Fluid Flow Projects) was used to simulate the flow in a horizontal well completed either circular perforations or slotted liners. Experiments were conducted with Reynolds numbers ranging approximately from 5,000 to 65,000 and influx to main flow rate ratios ranging from 1/50 to 1/1000. For both the perforation cases and slots cases, three different completion densities and three different completion phasings are considered.

Based on the experimental data, a new wellbore flow model for horizontal well was developed using the principles of conservation of mass and momentum.

ACKNOWLEDGMENTS

I would like to express my deepest appreciation to Dr. Cem Sarica, Professor of Petroleum Engineering at Penn State University and Dr. Mohan Kelkar, Professor of Petroleum Engineering at University of Tulsa, for their guidance and encouragement throughout my study here at TU. Thanks are also extended all the member companies of this research project, for their generous financial support.

I wish to thank Charles Ingle and Tony Butler, technicians of Tulsa University Fluid Flow Projects, for their technical support in instrumentation and facility maintenance. Thanks are also extended to Ginny Bentley for her secretarial work and Dr. Hong Yuan for her help in experiment design and flow modeling.

Finally I wish to say thanks to Dr. Ovadia Shoham and Dr. Erdal Ozkan for serving on the thesis committee.

TABLE OF CONTENTS

ABSTRACT iii

ACKNOWLEDGMENTS iv

TABLE OF CONTENTS v

LIST OF TABLES vi

LIST OF FIGURES viii

1. INTRODUCTION 1

2. LITERATURE REVIEW 6

3. EXPERIMENTAL PROGRAM 15

3-1. Flow Loop 15

3-2. Test Section 16

3-2.1. Multiple Slot Test Sections 16

3-2.2. Multiple Perforation Test Sections 17

3-3. Instrumentation and Data Acquisition 18

3-4. Experimental Procedure 21

4. MODEL DEVELOPMENT 23

5. RESULTS AND DISCUSSION 30

5-1. Multiple Slot Cases 30

5-1.1. Data Analysis Procedure 30

5-1.2. Experiments and Modeling 32

5-1.3. Discussions 37

5-2. Multiple Perforation Cases 41

5-1.1. Experiments and Modeling 41

5-1.2. Discussions 47
5-3. Evaluation of the Correlations 50
5-4. Parameters Affecting Apparent Friction Factor 55
6. CONCLUSIONS AND RECOMMENDATIONS 57
6-1. Conclusions 57
6-2. Recommendations 58
7. NOMENCLATURE 60
8. REFERENCES 63
APPENDIX: EXPERIMENTAL DATA 66

LIST OF TABLES

Table	Description	Page
3-1	Matrix for Multiple Slots Cases	17
3-1	Matrix for Multiple Perforation Cases	18
3-3	List of Instrumentation	20
5-1	a, b and C_n for the 7 Multiple Slots Cases	37
5-2	a, b and C_n for the 9 Multiple Perforation Cases	45
A-1	Experimental Data for Test Section 1	66
A-2	Experimental Data for Test Section 2	67
A-3	Experimental Data for Test Section 3	68
A-4	Experimental Data for Test Section 4	69
A-5	Experimental Data for Test Section 5	70
A-6	Experimental Data for Test Section 6	71
A-7	Experimental Data for Test Section 7	72
A-8	Experimental Data for Test Section 8	73
A-9	Experimental Data for Test Section 9	74
A-10	Experimental Data for Test Section 10	75

LIST OF FIGURES

Figure	Description	Page
1-1	Infinite Conductivity and Uniform Influx Assumptions and Comparison with Field Examples	2
2-1	Radial Velocity at Pipe Wall Due to Influx	8
2-2	Control Volumes for Momentum Equation and Energy Equation	9
3-1	Schematic of Test Facility	16
3-2	Schematic of the Test Sections and U-tube Manometer Connections	18
3-3	Instrumentation and Data Acquisition Flow Chart	19
4-1	Schematic of Horizontal Well Control Volume for Uniformly Distributed Injection Points	23
5-1	Experimental Data for Test Section 1	33
5-2	Experimental Data for Test Section 2	33
5-3	Experimental Data for Test Section 3	34
5-4	Experimental Data for Test Section 4	34
5-5	Comparison of Experimental Data for Three Phasings 1	38
5-6	Comparison of Experimental Data for Three Phasings 2	38
5-7	f_w vs. N_{Re} for Multiple Slots Cases	40
5-8	Comparison of Experimental Data for Three Densities	40
5-9	Experimental Data for Test Section 5	42
5-10	Experimental Data for Test Section 6	42
5-11	Experimental Data for Test Section 7	43
5-12	Experimental Data for Test Section 8	43
5-13	Experimental Data for Test Section 9	44

5-14 Experimental Data for Test Section 10 44
5-15 f_w vs. N_{Re} for Multiple Perforation Cases 46
5-16 Comparison of Experimental Data for Three Phasings 3 48
5-17 Comparison of Experimental Data for Three Phasings 4 48
5-18 Comparison of Experimental Data for Three Densities 1 49
5-19 Comparison of Experimental Data for Three Densities 2 49
5-20 Comparison of Different Correlation Predictions for Test Section 6 with Ratio 1/50 51
5-21 Comparison of Different Correlation Predictions for Test Section 6 with Ratio 1/1000 51
5-22 f_w vs. N_{Re} for Different Models 52
5-23 f_w / f_{w0} vs. N_{Rew} for Different Models 52
5-24 Comparisons of Correlation Predictions and Experimental Data 54

2. LITERATURE REVIEW

Horizontal wells are among the newest technologies in the recovery of gas and oil. In the long history of exploration and production of petroleum fluids, horizontal wells have been quite "neglected" until the latter half of this century. The petroleum industry started to investigate horizontal wellbore hydraulics in the late 1980's. Only in this decade have horizontal wells and related technology been received extensive attention. However the flow behavior in the velocity profile developing region, the flow behavior of porous pipes with fluid injection from the wall and the flow behavior in a distributing manifold, which are similar to the horizontal wellbore flow configuration, have been investigated in other disciplines. Following is a brief summary of pertinent studies.

The apparent friction factor for steady, incompressible flow in the laminar entry region of a smooth tube was first studied both experimentally and theoretically by Shapiro *et al.* (1954). In their study, the apparent friction factor is expressed as the skin friction coefficient plus a term representing the longitudinal rate of increase in momentum influx. The latter effect is associated with the developing velocity profile. It was concluded that nearly two thirds of all the pressure loss is caused by momentum changes.

Two years later, Yuan *et al.* theoretically investigated the effect of uniform injection at the wall on two-dimensional steady-state laminar flow in a porous-wall pipe. They solved the Navier-Stokes equations in cylindrical coordinates with appropriate

boundary conditions for small and large Reynolds numbers. The results showed that the effect of injection at the porous wall was to increase the friction coefficient at the wall.

Hornbeck *et al.* (1963) analytically studied the inlet region for laminar flow in porous pipes with small injection and suction. The velocity profile development was studied for both uniform and parabolic axial velocity profiles at the pipe inlet. They concluded that the centerline velocity for both inlet profiles with fluid injection approached the fully developed value at the same location.

Kinney (1968) examined the frictional characteristics of fully developed laminar flow in porous tubes with uniform mass transfer (Figure 2-1). He presented an equation to calculate friction coefficient which contains wall friction effects as well as those due to changes in axial momentum influx. The proposed equation, which was valid when N_{Rew} is no greater than 2, was

$$C_f N_{\mathrm{Re}} = 16\left[1 + \frac{N_{\mathrm{Re}\,w}}{24} - \frac{13}{2160}\left(N_{\mathrm{Re}\,w}\right)^2\right] \tag{2-1}$$

where:

C_f = wall friction coefficient (Fanning);

N_{Re} = axial Reynolds number;

N_{Rew} = wall Reynolds number,

$$N_{\mathrm{Re}\,w} = \frac{V_w \cdot d}{\nu} \tag{2-2}$$

where

d = pipe diameter;

V_W = radial velocity at wall;

ν = kinematic viscosity.

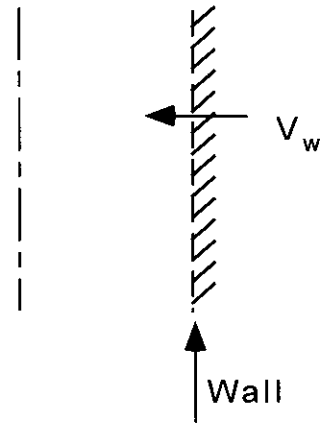

Figure 2-1: Radial Velocity at Pipe Wall Due to Influx

Olson and Eckert (1966) experimentally studied turbulent flow in a porous circular pipe with uniform air injection through the tube wall. Their experiments indicated that local friction factors were reduced by injection to an extent that they could be less than the friction factors in an identical pipe with no perforations when the injection to main flow velocity ratios reached a certain value and above.

Denn (1980) discussed flow and pressure distribution in a distributing manifold. He mentioned that this problem can not be solved exactly, but by use of the momentum and energy balances considerable insight can be obtained. First, he applied momentum equation to flow past a single port as shown in Fig. 2-2 (a). The dashed region is the

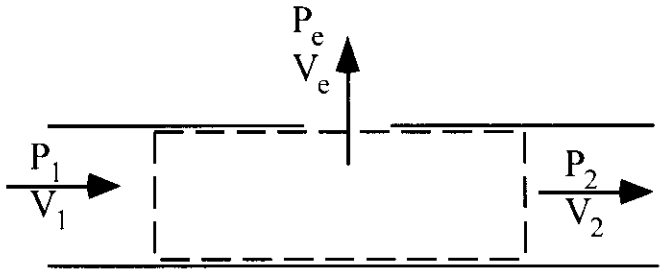

(a) Control Volume for Momentum Equation

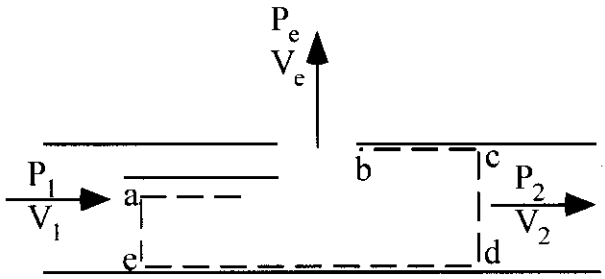

(b) Control Volume for Energy Equation

Figure 2-2: Control Volumes for Momentum Equation and Energy Equation

control volume. The pressure difference between sections 1 and 2 is then obtained as follows:

$$p_2 - p_1 = \rho (V_1^2 - V_2^2) \tag{2-3}$$

by neglecting the small frictional force on the tube wall from one side of the hole to the other and assuming that the flow V_e through the side hole is perpendicular to the direction of flow, in which case the side flow contains no axial momentum. Then he applied energy equation to this problem with the control volume shown in Fig. 2-2 (b). With the assumptions of 1) no flow across the line ab; 2) all fluid which flows across line cd enters the control volume across line ae and 3) no losses, the engineering Bernoulli equation applied to the control volume abcdea for a horizontal pipe simplifies to

$$p_2 - p_1 = \rho/2 (V_1^2 - V_2^2) \tag{2-4}$$

The estimate of pressure change given by energy equation is one-half that calculated from the momentum equation and it is not evident which is the more accurate.

As mentioned earlier, the Petroleum Industry began the investigation of horizontal wellbore hydraulics around a decade ago. The pioneer work was presented by Dikken in 1989. Dikken proposed a simple analytical model for turbulent flow under the assumptions of single phase flow in the wellbore and a steady state fluid flow in the reservoir. He described the flow in the reservoir with a specific productivity index, which is independent of position along the well. A differential equation was developed that can be solved for flow rate distribution along the wellbore. Dikken gave solutions for cases

of both infinite and finite well length. The friction factors in this paper were calculated by regular pipe friction factor correlations.

Seines (1990) experimentally studied the roughness of slotted liners, and a value of 0.4 - 0.8 mm was reported. Novy (1992) used this value to compute the frictional pressure drop in horizontal wellbores completed with slotted liners. He gave a criterion to evaluate the effect of wellbore friction on well length, production rate and well diameter for smooth and rough pipes. His studies indicated that, when the ratio of wellbore pressure drop to drawdown exceeds 10-15%, then the wellbore friction can reduce productivity by 10% or more. This could be the case for oil wells producing more than 1,500 STB/D and gas wells producing more than 2 MMscf/D.

Asheim *et al.* (1992) conducted an experimental and theoretical study. They proposed the following new friction factor for horizontal wellbores, which includes accelerational pressure losses due to continuous fluid influx along the wellbore.

$$f = f^o + 4d\left(\frac{q_L}{q}\right) + 2\frac{d}{n}\left(\frac{q_L}{q}\right)^2 \qquad (2\text{-}5)$$

where:

f^o = wall friction factor, as for regular unperforated pipe;

d = pipe diameter (m);

n = perforation density (m^{-1});

q_L = inflow rate per length unit ($m^3/s/m$); and

q = pipe flow rate (m^3/s).

In deriving this equation, they assumed that the injected fluid enters the main flow with no momentum in the axial direction. Their experimental results were for one perforation and two perforations separated by a 200-mm length, and for Reynolds numbers between 14,000 and 86,400.

Kloster (1990) experimentally studied flow resistance in perforated pipe, both with fluid injection and without fluid injection. The Reynolds numbers covered in his experiments ranged from 60,000 to 450,000. He concluded that the friction factor vs. Reynolds number relationship for perforated pipes with no injection from the perforations did not show the characteristics of regular pipe flow. The friction factor was 25~70% higher than that of regular commercial pipes. He also observed that small injection reduced the friction factor.

Ozkan *et al.* (1992, 1993) presented a semi-analytical model that coupled wellbore and reservoir fluid flow, and incorporated the effect of laminar and turbulent flow regimes in the wellbore. They showed that wellbore hydraulics influence horizontal well productivity. Regular pipe friction factor correlations were used in their study.

Brekke (1992) studied the effect of completion methods on horizontal well productivity and reported that frictional pressure loss due to restricted flow through perforations reduces the productivity of wells. A field test in the North Sea using this completion technique also showed reduced frictional pressure losses in horizontal wellbores.

Su and Gudmundsson (1993 and 1994) proposed an empirical friction factor correlation for perforated pipes without fluid injection from the perforations. They found that the total pressure drop along the horizontal wellbore consists typically of 80 percent wall friction, 15 percent mixing effect (including perforation roughness) and 5 percent pressure drop due to acceleration.

Ouyang *et al.* (1996 and 1998) investigated both single phase and two phase flow behaviors in horizontal wells. They developed a wellbore model which they claimed can be readily used under different wellbore perforation patterns and well completion conditions. However, they assumed uniform wall shear stress for different perforation patterns and well completions which may not be necessarily true. And they didn't incorporate the effects of perforation distribution into their friction factor correlation. A local friction factor correlation was developed to be used for the wellbore flow rate before the perforation point either zero or none zero. However, according to Olson and Eckert (1966), the phenomena is quite different for zero velocity at the beginning of porous pipe case. Ouyang *et al.* also mentioned that for turbulent flow, inflow reduces the wall friction, while other investigators (Kato *et al.* 1993, Yuan 1997, Yuan et al. 1996) found that inflow could reduce or increase wall friction depending on influx rates and injection opening distributions.

Yuan (1994, 1996, 1997) conducted around 1000 experimental tests investigating the flow behavior in horizontal wells with single opening, perforated horizontal wells and horizontal wells completed with multiple slot liners. By using the principles of mass and momentum conservation, general horizontal well friction factor expressions were developed for both the perforated horizontal wells and horizontal wells completed with

slot liners. Horizontal well friction factor correlations were developed by applying experimental data to the general friction factor expressions. It was observed that the friction factor for a perforated pipe with fluid injection could be either smaller or greater than that for a smooth pipe, depending on perforation densities and influx to main flow rate ratios. The proposed friction factor correlation can be used in any horizontal well model which considers pressure variation along the wellbore.

The results of Yuan's studies suggest that the shape and the distribution of the openings on the wellbore surface can significantly influence the flow behavior in a horizontal well. Each completion geometry displays different flow characteristics. In Yuan's studies, a general friction factor correlation was developed to predict the pressure loss along the horizontal wellbore when the operation conditions are dynamically similar to those of the experiments. However, because the available data consider either single opening or limited multiple opening cases, the influence of the shape and the area of the openings has not been thoroughly investigated. Yuan's theoretical approaches were used in this study and her experimental data were incorporated into the horizontal wellbore hydraulics modeling.

3. EXPERIMENTAL PROGRAM

An existing small-scale test facility at TUFFP (Tulsa University Fluid Flow Projects) was modified to simulate the flow behavior in horizontal wells completed with either circular perforations or slotted liners. The test facility is composed of three major parts: a flow loop, a test section and an instrumentation center. The flow loop consists of the fluid handling system (water tank, the centrifugal pump and the screw pump), the metering sections (turbine meters, temperature transducers, pressure transducers) and flow control sections (control valves). The test section includes the instrumentation for measuring pressure differences. The instrumentation center houses a patch panel, signal conversion circuitry and a computer based data acquisition system.

3-1. the Flow Loop

The flow loop is composed of three major parts, the fluid handling system, the metering sections and the flow control sections. A schematic description of the test facility is given in Fig. 3-1.

Water is used as the testing fluid and is stored in a 200 gal (0.757 m^3) steel tank which provides water for both the main flow and the side flow. A centrifugal pump and a screw pump are used to supply and control the main flow and side flow rates, respectively. Filters are placed downstream of the pumps and upstream of the metering sections to remove particles in the water and protect the turbine meters. Each metering section is composed of three turbine meters which can be used to measure different

ranges of flow rate, and a temperature transducer for measuring fluid temperature. The turbine meters are calibrated using a weighing tank, and temperature transducers are calibrated using a thermal bath and a thermometer. The water flows through the test section and is then circulated back to the steel storage tank. This results in a constant liquid level in the tank without using a constant level regulator, permitting long test times.

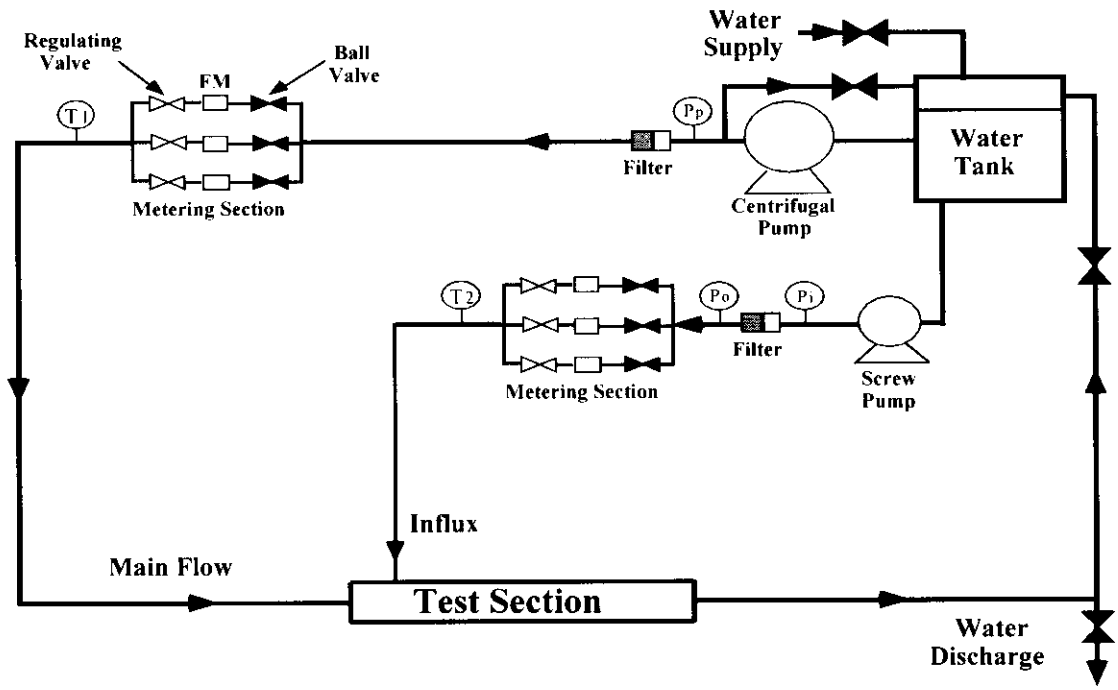

Fig. 3-1: the Schematic of the Test Facility

3-2. Test Section

3-2.1 Multiple Slots Test Sections

Four test sections were used. They are 10-ft long, one-inch diameter plastic pipes with the 4-ft long multiple slots section located in the middle of each pipe. The total numbers of slots in the test sections are 12, 18 and 36 with phasings of 360°, 180°, and 90° (see Table 3-1 for the combinations of slots densities and phasings). All those cases

denoted by X were investigated by Jasmine Yuan and all those cases denoted by √ were investigated in this study). The slots have dimensions of 2. in. in length and 1/16 in. in width. The test section is covered with about 50 layers of cloth to ensure uniform influx since the pressure loss through the cloth will be much greater than the pressure loss inside the 1-in. diameter pipe or in the annulus through which liquid feeds the influx openings.

Table 3-1: Matrix for the Multiple Slots Cases (Slot liner Dimensions: Length: 2 in., Width: 1/16 in.)

Slot Liners Density	Slot liners Phasing		
	360	180	90
Single Opening			
18 slots/4 ft	X	X	√
12 slots/4 ft		√	√
36 slots/4 ft		√	X

There are four pressure ports along each test section (Fig. 3-2). The distance between the test section starting point and pressure port No. 1 is greater than 2 ft, which allows the flow to fully develop. The pressure differences along the test section length were measured by 4 U-tube manometers. Carbon tetrachloride was chosen as the manometer fluid due to its low density. The pressure difference between the inner pipe and the annulus is measured by a pressure transducer.

3-2.2 Multiple slot Test Sections

Six perforated test sections were used. The perforation densities investigated in this study are 5, 10 and 20 shots per foot and the perforation diameters are all the same, equal to 1/8 in. (geometrically similar to a 6-in. diameter casing with a perforation diameter of 3/4 in.) The perforations are uniformly distributed along the pipes with the phasings of 360°, 180°, and 90° (see Table 3-2 for the combinations of perforation

densities and phasings). Locations of pressure ports and pressure measurement devices are same for as those used in the multiple slots cases.

Table 3-2: Matrix for the Multiple Perforation Cases (Perforation Diameter: d=1/8 inch)

Perforation Density	Perforation Phasing		
	360	180	90
Single Opening	X		
5 shot/ft	X	√	√
10 shot/ft	√	X	√
20 shot/ft	√	√	X

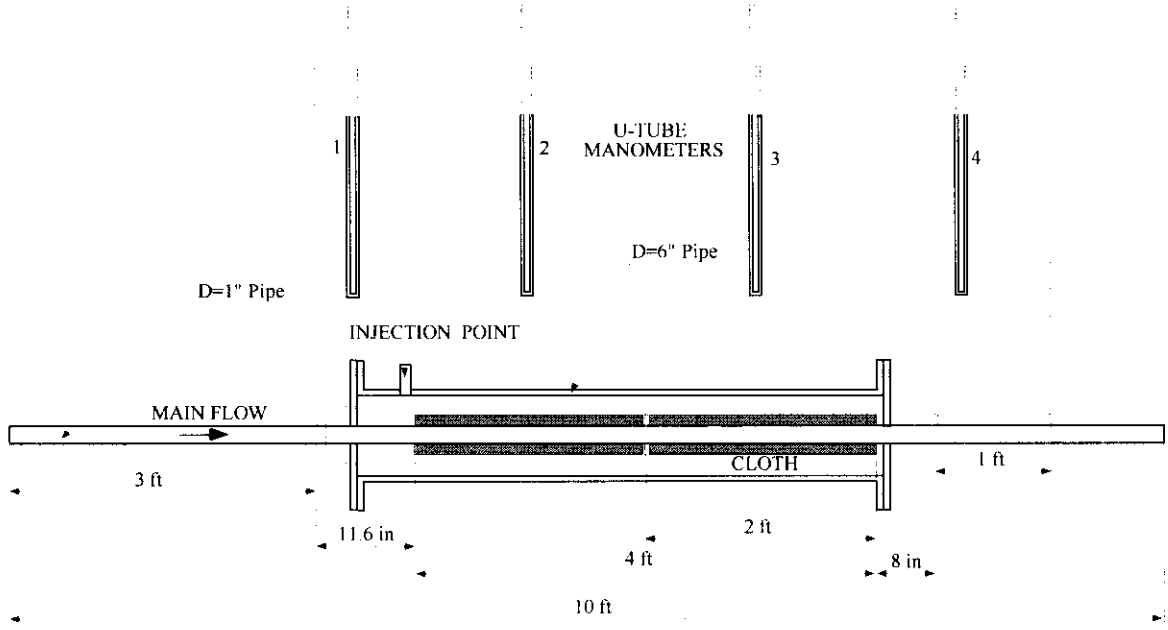

Figure 3-2: Schematic of the Test Section and U-tube Manometer Connections

3-3. Instrumentation and Data Acquisition

A flow chart of the instrumentation and data acquisition system used is shown in Fig. 3-3. Table 3-3 gives a summary of the instrumentation used in the test facility.

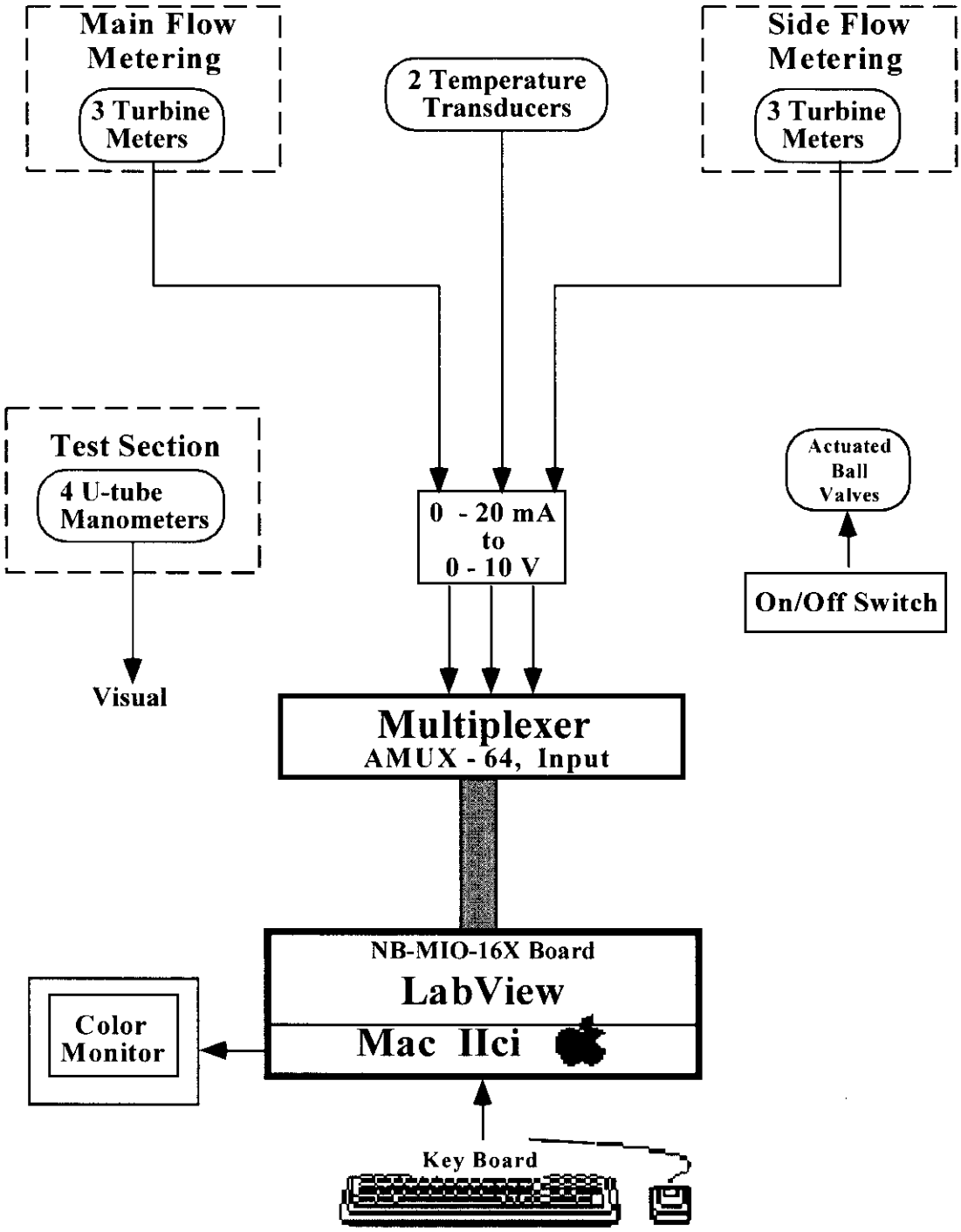

Figure 3-3: Instrumentation and Data Acquisition Flow Chart

Table 3-3: List of Instrumentation

Instrument	Range		Output
Turbine Meters			
FM1	0.125 - 3.0	GPM	0-10 V
FM2	0.5 - 5.0	GPM	0-10 V
FM3	2.0 - 60.0	GPM	0-10 V
FM4	0.125 - 3.0	GPM	0-10 V
FM5	0.5 - 5.0	GPM	0-10 V
FM6	1.5 - 15.0	GPM	0-10 V
Pressure Measurements			
U-tube Manometers	Δh_{max} = 600mm H_2O Column		Visual
Pressure Transducer	0 - 40 psi		0-10 V
Temperature Transducers			
TT1	40-160 ^{o}F		0-10 V
TT2	40-160 ^{o}F		0-10 V
Pumps			
Pump-Side (Screw Pump)	5.2 Gal /100 RPM		
Pump-Main (Centrifugal Pump)	Q_{max} = 99 GPM H_{max} = 93 FT		
Filter			
Filter-Side	Q_{max} = 45 GPM 2 Micron		
Filter-Main	Q_{max} = 56 GPM 2 Micron		

In the instrumentation center, output signals from turbine meters, temperature transducers and the pressure transducers are transmitted to a patch panel. The patch panel contains a Macintosh II Ci computer, the signal converters and power supplies. The output signalsare converted to 0-10 volt analog signals in the patch panel and routed to an input board which uses a National Instruments AMUX-64 multiplexer. A data acquisition board installed in the Macintosh computer provides 16 single-ended A/D channels, digital and analog outputs, and handles all the analog signal interfaces. A four-to-one multiplexer board was installed in the control cabinet to interface more instrument signals.

Experiments were conducted for steady state flow with Reynolds numbers ranging from approximately 4,000 to 65,000 and influx to main flow rate ratios ranging from 1/50 to 1/1000 for both the multiple perforation cases and the multiple slots cases. The influx to main flow rate ratios at different Reynolds numbers were determined based on uniform influx and infinite conductivity cases. Main flow rates, influx flow rates and pressure variations along the test section were measured. All measurements, with the exception of manometer readings, were collected using a LabVIEW data acquisition system with a Macintosh computer. The uniqueness of LabVIEW is that it uses front panel and block diagrams for building hierarchical virtual instruments. A virtual instrument is a software program package designed to look and act like a real instrument.

3-4. Experimental Procedure

The experimental procedure consists of the following steps:

1. Calibrate the turbine meters, temperature transmitters and pressure transducer. A unique linear relationship between the measured parameter and the output voltage can be obtained for each instrument.

2. Check the water level of the water tank.

3. Fully open the bypass valve. The bypass valve is used to protect the flow meters.

4. Start the centrifugal pump and close the bypass valve slowly until the pressure gauge indicates a reading of 35 psia.

5. Open the main flow valve gradually until the desired flow rate is reached.

6. Open the valves between U-tubes and test section, check the water/carbon tetrachloride interface in the U-tube manometers and making sure that there are no gas bubbles in the pipe.

7. Fully open screw pump bypass valve, start the screw pump and open the side flow valve untill the desired flow rate is reached.

8. After reaching steady state for each selected influx to main flow rate ratio, start the LabVIEW data acquisition system and take manometer readings.

9. After data acquisition, stop the screw pump and close the side flow valve.

10. Close the main flow valve. Stop the centrifugal pump and finally close the bypass valve slowly.

4. MODEL DEVELOPMENT

A general model developed by Jasmine Yuan, a former Ph.D student at University of Tulsa, has been adopted to predict friction factor for horizontal wells completed with multiple perforations or multiple slotted liners. Here, the development of the general model will be presented after Yuan.

Consider an incompressible fluid flowing isothermally along a uniformly perforated pipe of cross-section A. The area of each perforation is A_p. Fluid injected through the perforations into the main flow stream uniformly as illustrated by Figure 4-1.

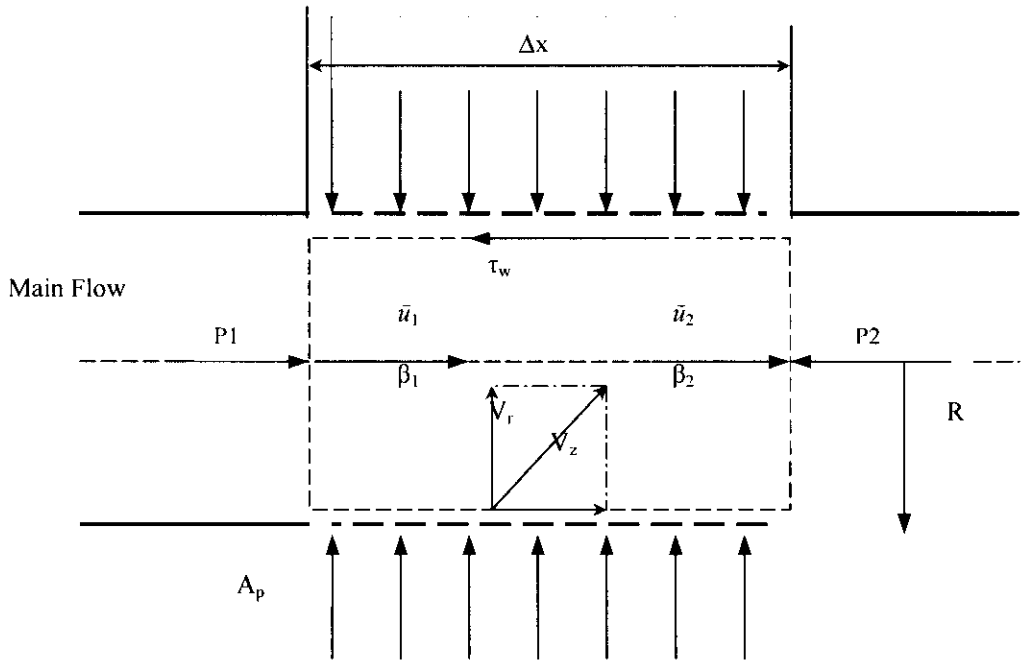

Figure 4-1: Schematic of Horizontal Well Control Volume for Uniformly Distributed Injection Points

When the injected fluid enters the main flow stream through the perforations, the streamlines change directions. Each local mean velocity is tangent to the streamlines and can be divided into two components, V_r and V_x. Fluid is transported into the main flow with a radial velocity component V_r, while retaining some axial momentum from velocity component V_x. The dotted lines define a control volume in which fluid is transported across surfaces A_1, A_2, and A_p. Assume there are n perforations along Δx.

The momentum balance for the control volume in axial direction is:

$$p_1 A - p_2 A - \tau_w \cdot \pi \cdot d \cdot \Delta x = \beta_2 \rho \bar{u}_2^{\,2} A - \beta_1 \rho \bar{u}_1^{\,2} A - \rho V_x V_r \beta_p A_p n \qquad (4\text{-}1)$$

p_1 and $\bar{u}_1$ are the pressure and average velocity at the inlet of the control volume respectively and p_2 and $\bar{u}_2$ are the pressure and average velocity at the exit respectively. For the three terms on the left-hand side of Eq. (4-1), we can assume that average properties completely define the flow field. The first two terms on the right hand side of the equation use the average velocities by introducing momentum correction factors, $\beta_1$and β_2, which are defined by the following equation:

$$\beta = \frac{1}{AV^2} \int_A u^2 dA \qquad (4\text{-}2)$$

In the last term of Eq. (4-1), we assume $V_r = V_p$, from continuity considerations. β_p is the momentum correction factor for the influx stream and V_x will be discussed later. We can further consider

$$A_1 = A_2 = A \qquad \text{and} \qquad \rho_1 = \rho_2 = \rho_p = \rho$$

For multiple injection openings, it is convenient to use average properties. The average velocity over Δx is $\bar{u}$ and is defined as follows

$$\bar{u}=(\bar{u}_1+\bar{u}_2)/2 \tag{4-3}$$

Mass balance for the control volume is given by

$$\bar{u}_1 A+nV_p A_p=\bar{u}_2 A \tag{4-4}$$

The influx rate through each perforation is

$$q_{in}=V_p A_p \tag{4-5}$$

The total volumetric influx rate is

$$Q_{in}=nV_p A_p \tag{4-6}$$

Velocity $\bar{u}_1$ and $\bar{u}_2$ in Eq. (4-1) may be eliminated by employing the following relationships,

$$\bar{u}_1=\bar{u}-\frac{n}{2}V_p\frac{A_p}{A} \tag{4-7}$$

$$\bar{u}_2=\bar{u}+\frac{n}{2}V_p\frac{A_p}{A} \tag{4-8}$$

Substituting Eq.s (4-7) and (4-8) into Eq. (4-1), dividing through by $A\Delta x$ and simplifying, yields

$$\frac{p_1 - p_2}{\Delta x} - \tau_w \frac{4}{d} =$$

$$\rho \bar{u}^2 \cdot \frac{\beta_2 - \beta_1}{\Delta x} + n\rho \bar{u} V_p \frac{A_p}{A} \cdot \frac{1}{\Delta x} \cdot (\beta_2 + \beta_1 - \frac{V_x}{\bar{u}} \beta_p) + \rho V_p^2 \cdot \frac{n^2}{4} \cdot \frac{A_p^2}{A_2} \cdot (\beta_2 - \beta_1) \cdot \frac{1}{\Delta x} \tag{4-9}$$

An apparent friction factor, defined as the ratio of the net imposed external forces to the inertial forces, can be given by:

$$f_T = -(\frac{p_2 - p_1}{\Delta x}) / \frac{\rho \bar{u}^2}{2d} \tag{4-10}$$

which is an average friction factor over a length Δx. Δx is the measured test section length plus a calculated flow developing length.

The wall friction factor f_W is defined as:

$$f_w = \frac{8\tau_w}{\rho \bar{u}^2}. \tag{4-11}$$

Let

$$\phi = \frac{V_x}{\bar{u}} \tag{4-12}$$

$$\varphi = \frac{n}{\Delta x} \tag{4-13}$$

In Eq. (4-13), φ is the density of injection openings. An expression for the apparent friction factor can then be found by substituting Eqs. (4-10) to (4-13) into Eq. (4-9),

$$f_T = f_w + 2d \cdot \left(\frac{\beta_2 - \beta_1}{\Delta x} \right) + 2d\varphi \cdot \frac{q_{in}}{\overline{Q}} \cdot \left[\beta_1 + \beta_2 - \phi\beta_p + \left(\frac{n}{4} \cdot (\beta_1 - \beta_2) \cdot \frac{q_{in}}{\overline{Q}} \right) \right] \tag{4-14}$$

Let

$$C_n = \left[\beta_1 + \beta_2 - \phi\beta_p + \left(\frac{n}{4} \cdot (\beta_1 - \beta_2) \cdot \frac{q_{in}}{\overline{Q}} \right) \right] \tag{4-15}$$

Eq. (4-14) becomes:

$$f_T = f_w + 2d \cdot \left(\frac{\beta_2 - \beta_1}{\Delta x} \right) + C_n 2d\varphi \cdot \frac{q_{in}}{\overline{Q}} \tag{4-16}$$

where C_n must be determined from experiments. Each term at the right hand side of Eq. (4-16) is discussed later.

Based on Buckingham π theorem, the apparent friction factor is a function of wall friction factor, Reynolds number, the influx to main flow ratio, the axial component of the influx velocity to average main flow velocity ratio, completion geometry, perforation or slot size, density and phasing. (For detailed derivation, see Hong Yuan's Ph.D. dissertation Appendix A)

$$f_T = f\left(f_w, N_{\mathrm{Re}}, \frac{q_{in}}{\overline{Q}}, \phi, \frac{A_p}{A}, \varphi d, \alpha \right) \tag{4-17}$$

The first term on the right hand side of Eq. (4-16) is the wall friction factor. One should realize that the wall friction factor definition is due to no momentum change in the control volume. The wall shear stress term in Eq. (4-11), τ_W, can be quite different from

that of regular pipe flow. Nevertheless, the same form of wall friction factor is adopted here for simplicity. The wall shear stress in Eq. (4-11) is defined as $\tau_w = -\mu \left.\frac{du}{dr}\right|_{r=R}$. Therefore, f_w reflects the velocity profile change in the radial direction near the pipe wall. Fluid injection will influence velocity profiles directly; therefore, it will influence the value of f_w. At small injection rates, according to the literature, the boundary layer will be lubricated and f_w will decrease to a value that is less than the friction factor for the no fluid injection case.

The second term on the right hand side of Eq. (4-16), $2d \cdot \frac{\beta_2 - \beta_1}{\Delta x}$ is caused by a change in the velocity profile in the axial direction. For small injection rates, this term is negligible since the injected fluid will not affect the velocity field significantly, except in the near wall region. If velocities at both cross sections are fully developed, the term is negligible. If we use the Blasius formula to approximate the wall friction factor, then Eq. (4-16) becomes,

$$f_T = aN_{\mathrm{Re}}^b + C_n \cdot 2d\varphi \cdot \frac{q_{in}}{\bar{Q}} \tag{4-18}$$

where a, b, C_n will be determined experimentally and expressed in terms of the perforation density φ and the perforation phasing α.

For small influx to main flow rate ratios, or no severe velocity profile changes, $C_n=\beta_1+\beta_2-\phi\beta_p$. If the injected fluid enters the main flow with no momentum in the axial direction, i. e. $V_x=0$, then $\phi\beta_p$ in Eq. (4-16) is equal to zero, and $C_n=\beta_1+\beta_2$. If we further

assume that $\beta_1=\beta_2=1$, $C_n=2$. If the injected fluid is considered to have a velocity of $\bar{u}$ once it enters the main flow stream, i. e. $V_x=\bar{u}$, then the ϕvalue in Eq. (4-16) becomes 1, and therefore $C_n=\beta_1+\beta_2-\beta_p$.

5. RESULTS AND DISCUSSIONS

Ten test sections were used during the experiments and a large number of experimental data were acquired. All the experimental data were given in Appendix. In this chapter, the data analysis procedure and experimental data for each test section are given. Also given are the parameters affecting apparent friction factor and comparisons of the derived apparent friction factor correlation to other correlations in the literature.

5-1. Multiple Slot Cases

A total of 360 experimental tests are conducted for the four multiple slots test sections as described in Chapter 3. Since we have already had very good qualitative understanding of the wellbore hydraulics in completed horizontal wells from Yuan's study, no tests were conducted to acquire data for the no fluid injection case or no main flow at the inlet of the test section case. Tests were conducted for the fluid injection case with Reynolds numbers ranging approximately from 5,000 to 65,000 and influx to main flow rate ratios varying from 1/50 to 1/1000 (For the second test section, a ratio of 1/800 was used instead of 1/1000). All the experiments were conducted in room temperature (usually ranging from 75 ^{o}F to 85 ^{o}F). In this section, data analysis, experiment results and discussions are presented.

5-1.1. Data Analysis Procedure

The parameters measured in this study are influx and main flow rates, influx and main flow temperatures, and pressure variations along the test section and the pressure

differences between the inner pipe and annulus. For multiple slot cases, it is convenient to use average properties to analyze the data.

First we use the following equation to calculate the average Reynolds number:

$$N_{\mathrm{Re}} = \frac{\rho \bar{u} d}{\mu} \tag{5-1}$$

For fully developed flow, regular pipe friction factor correlations can be used to calculate the friction factor. For the flow region affected by radial influx, the apparent friction factor f_T is calculated from the pressure drop, the distance, and the flow rate defined below:

$$f_T = \frac{\Delta p / \Delta x}{\rho \bar{u}^2 / 2d} \tag{5-2}$$

where

Δx = distance between one pipe diameter upstream of the slotted section and L_d downstream of the slot;

L_d = the flow developing length calculated using CFD simulation results (see Eq. 5-3);

Δp = pressure drop over Δx;

$\bar{u}$ = flow velocity calculated by $\bar{u} = \frac{4(Q_1 - Q_{in}/2)}{\pi d^2}$;

Q_{in} = total influx rate along the slotted section, $Q_{in}=n\ q_{in}$;

q_{in} = influx rate from one slot;

ρ, μ = water density and viscosity, changing with temperature;

d = pipe diameter.

The correlation to predict the flow developing length at various Reynolds numbers and injection to main flow velocity ratios was developed by Yuan *et al.* based on the their CFD simulation results:

$$L/d = a\ log(V_{in}/V) + b \tag{5-3}$$

where $$a = 3.790\times10^{-4}\left(N_{Re}/1000\right)^2 + 5.213\times10^{-3}\left(N_{Re}/1000\right) + 0.753 \tag{5-4}$$

$$b = 8.173\times10^{-4}\left(N_{Re}/1000\right)^2 + 2.593\times10^{-3}\left(N_{Re}/1000\right) + 5.139 \tag{5-5}$$

5-1.2. Experiments and Modeling

Figure 5-1 through 5-4 show the variations in apparent friction factor with influx to main flow rate ratios and Reynolds numbers for the four test sections with multiple slot completions. Each figure is plotted as apparent friction factor f_T vs. Reynolds number N_{Re}, and the different data series represent experimental results at different influx to main flow rate ratios. As we can see from the figures, in most test sections the f_T is greater than the smooth pipe friction factor calculated from the Blasius formula for all influx to main flow rate ratios. When the influx to main flow rate ratio approaches zero, the f_T vs. N_{Re} curve will move closer to the curve predicted by the Blasius formula.

Lubrication effects were found for the first test section when the influx over main rate ratio is 1/1000. In all the cases, the f_T decreases considerably with the decreasing of influx to main flow rate ratio at high flow rate ratio cases. However the decrease of the friction factor is negligible at very low influx/main flow rate ratios. We can predict that the friction factor will approach a constant at very small influx over main flow ratios. The relationship of the friction factor and the Reynolds number of a completed horizontal

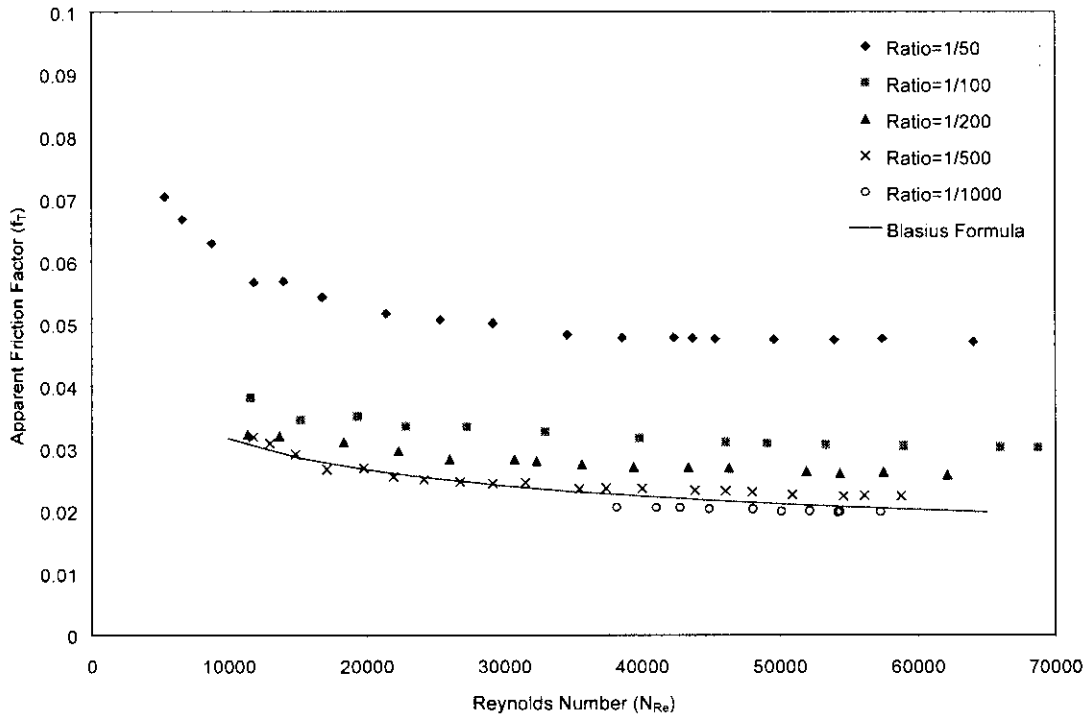

Fig. 5-1: Experimental Data for Test Section 1 (Slots, 4.5 slots/ft with 90° phasing)

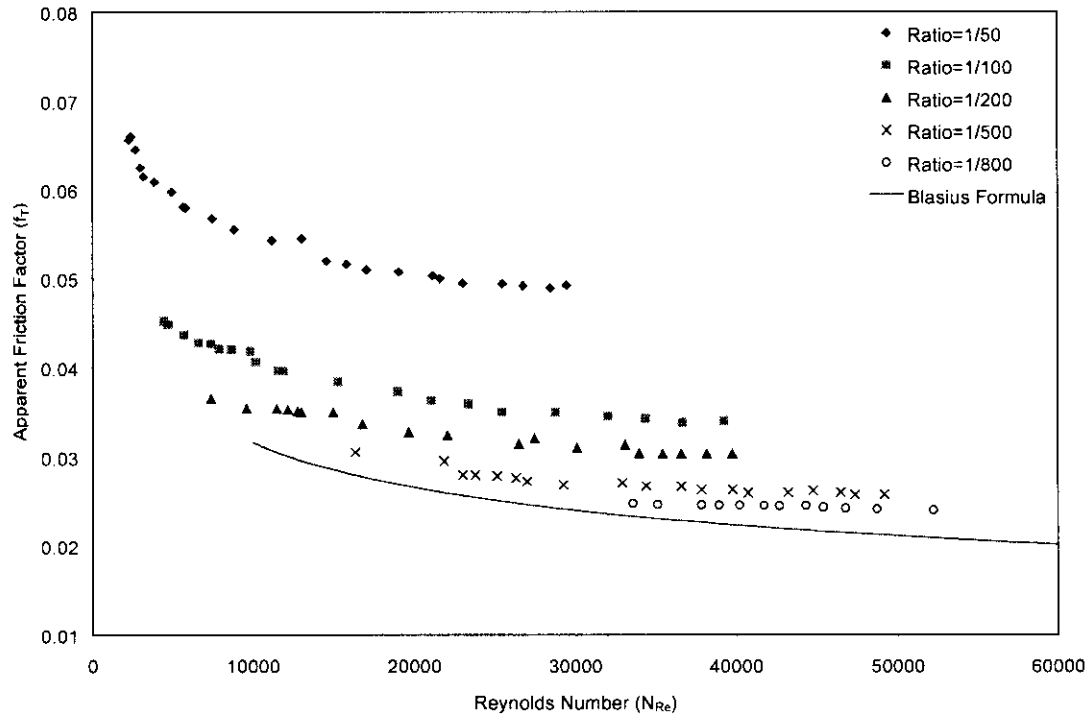

Fig. 5-2: Experimental Data for Test Section 2 (Slots, 3 slots/ft with 180° phasing)

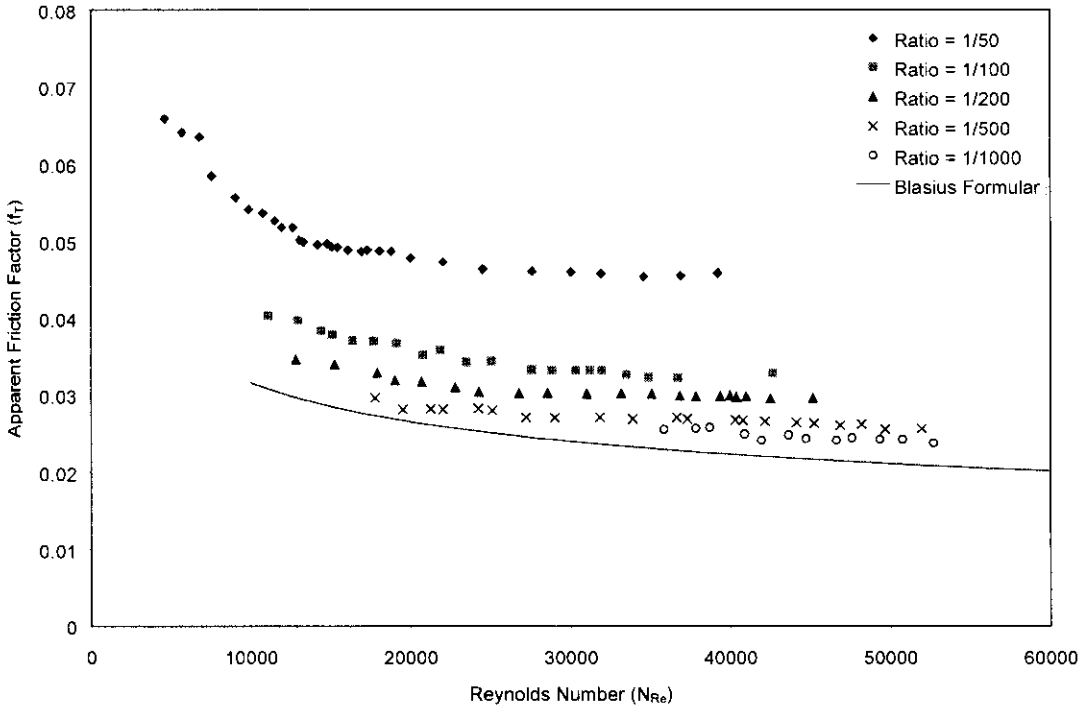

Fig. 5-3: Experimental Data for Test Section 3 (Slots, 3 slots/ft with 90° phasing)

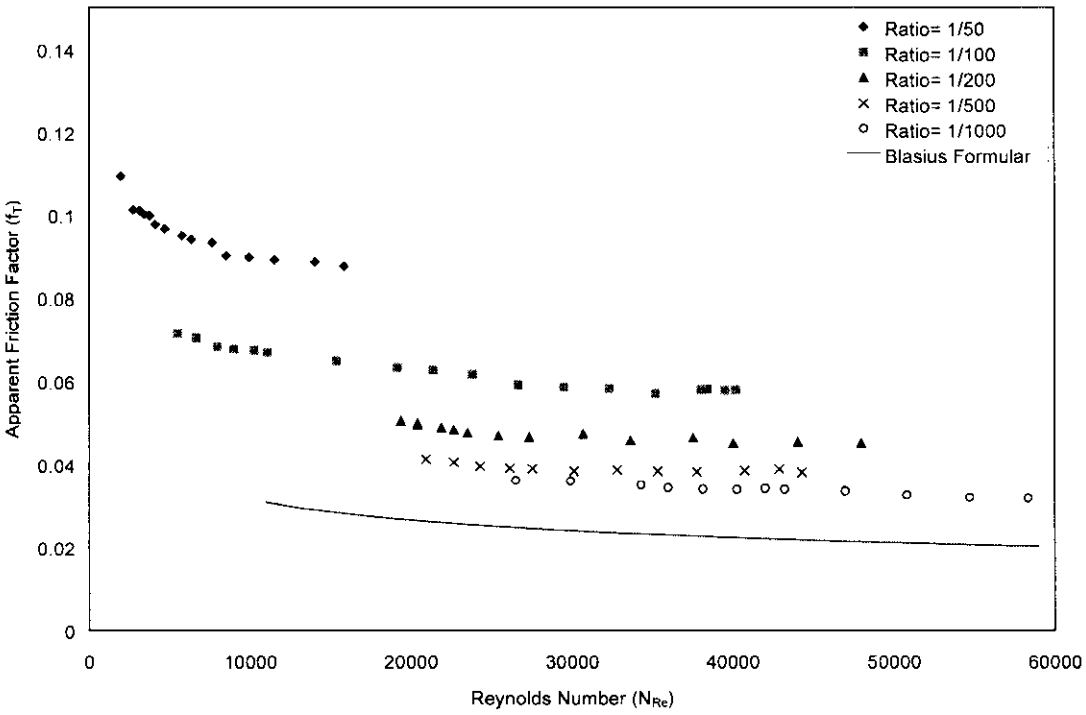

Fig. 5-4: Experimental Data for Test Section 4 (Slots, 9slots/ft with 180° phasing)

wellbore may have different characteristics other than those of regular horizontal pipes, nevertheless in both cases the friction factors exhibit the same behaviors at high Reynolds numbers. For a given flow rate ratio, f_T decreases with the increasing of Reynolds number. (f_T always approaches a near constant once the Reynolds number exceeds 40,000.) For a given completion density, f_T is always the smallest when the phasing is 90^0.

The experimental data were used to determine a, b and C_n in the following equation

$$f_T = aN_{\mathrm{Re}}^{b} + C_n \cdot 2d\varphi \cdot \frac{q_{in}}{\overline{Q}} \tag{5-6}$$

where a, b and C_n are functions of momentum correction factors β_1, β_2 and β_p, influx to main flow flow ratio, the completion phasing α and the completion density φ. And β_1, β_2 and β_p themselves are functions of all the above parameters. From Yuan's study, it's known that both the completion phasing α and the completion density φ have far more impacts on a, b and C_n than the influx to main flow rate ratio especially when the influx over main flow rate ratio is quite small. Thus in the data analysis procedure, regression analysis is applied first to each data set and get averaged a, b and C_n for all the different influx to main flow rate ratios. Then regression analysis is used again to express a, b and C_n in terms of the remaining parameters α and φ.

Table 5-1 lists all the a, b and C_n in the first step of the data analysis procedure. Applying regression analysis, the following expression have been obtained for a, b and C_n.

a: *a* is in the range of 0.17 to 1.14. The following correlation can be used to estimate the a value:

$$a = -0.611656 + 0.0651749\varphi + \frac{84.2771}{\alpha} \tag{5-7}$$

b: *b* is in the range of -0.19 to -0.37. At medium completion density and high phasing, b value is very close to –0.25 in the Blasius formula. Eq. (5-8) can be used to estimate the value for b:

$$b = -0.198817 + \frac{1.41439}{(\varphi - 4.5)^2 + 16.0191} - \frac{12.7926}{\alpha} + 0.000133823\varphi \tag{5-8}$$

C_n: In our study, the value of C_n is in the range of 1.76 to 2.4. The following equation can be used to get an estimated C_n when the completion density and phasing are known:

$$C_n = 2.25 - 0.0161188\varphi + \frac{12.9954}{\alpha} \tag{5-9}$$

It should be pointed out that at higher N_{Re} (when N_{Re} is greater than 40,000), the first term on the left hand side of Eq. 6-3 for those cases with 360° phasing is very close to the Blasius formula $0.316(N_{Re})^{-0.26}$. At same time, the second term on the left-hand side of Eq. 5-6 usually is the dominant term at high Reynolds numbers. It means that at those situations the Blasius formula for regular pipes can be used directly to approximate the wall friction factor f_w without introducing too much error (the error due to this approximation is usually 5-10% for the apparent friction factor).

The above correlation results can be incorporated into horizontal well simulation models in order to calculate the pressure drop through the whole production system. For special cases when the perforation parameters are known and those parameters are closer to those we have investigated in our experiments, a, b and C_n can be read directly from the Table 5-1 which will give more accurate results than those obtained using the correlations.

Table 5-1: a, b and C_n for the 7 Multiple Slots Cases

	α	φ (slots/ft)	a	b	C_n
1	90	3	0.392936	-0.266344	1.999548
2	180	3	0.171137	-0.18886	2.41148
3	90	4.5	0.130379	-0.174987	1.78065
4	180	4.5	0.312526	-0.258063	2
5	360	4.5	0.340384	-0.256828	2.2
6	90	9	1.14138	-0.37462	2.3
7	180	9	0.172403	-0.15582	1.76806

5-1.3 Discussions of Effects of the Slots Phasing and Density upon the Pressure Drop Behavior

In this study, extensive experiments have been conducted to investigate the effects of the completion phasing upon the liquid behavior in horizontal wells. As we can see from Figure 5-5 and Figure 5-6, other parameters being equal, the decreasing of the completion phasing from 360° to 180° and then to 90° decreases the total friction factor.

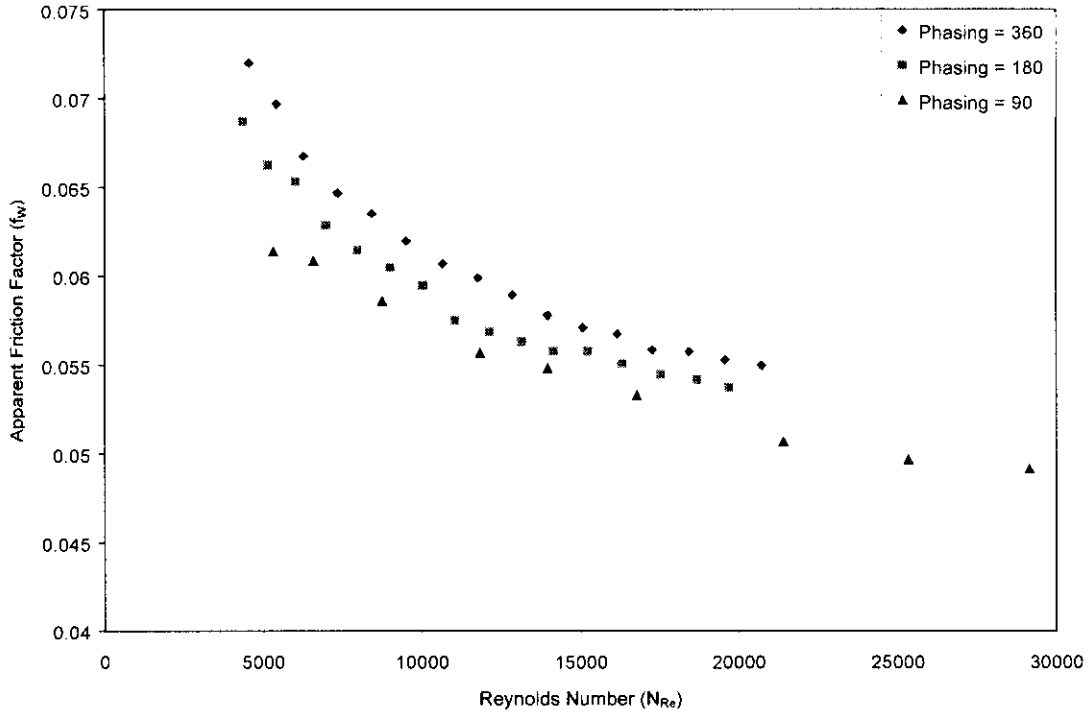

Figure 5-5: Comparison of Experimental Data for Three Phasings (φ = 4.5 slots/ft, ratio = 1/50)

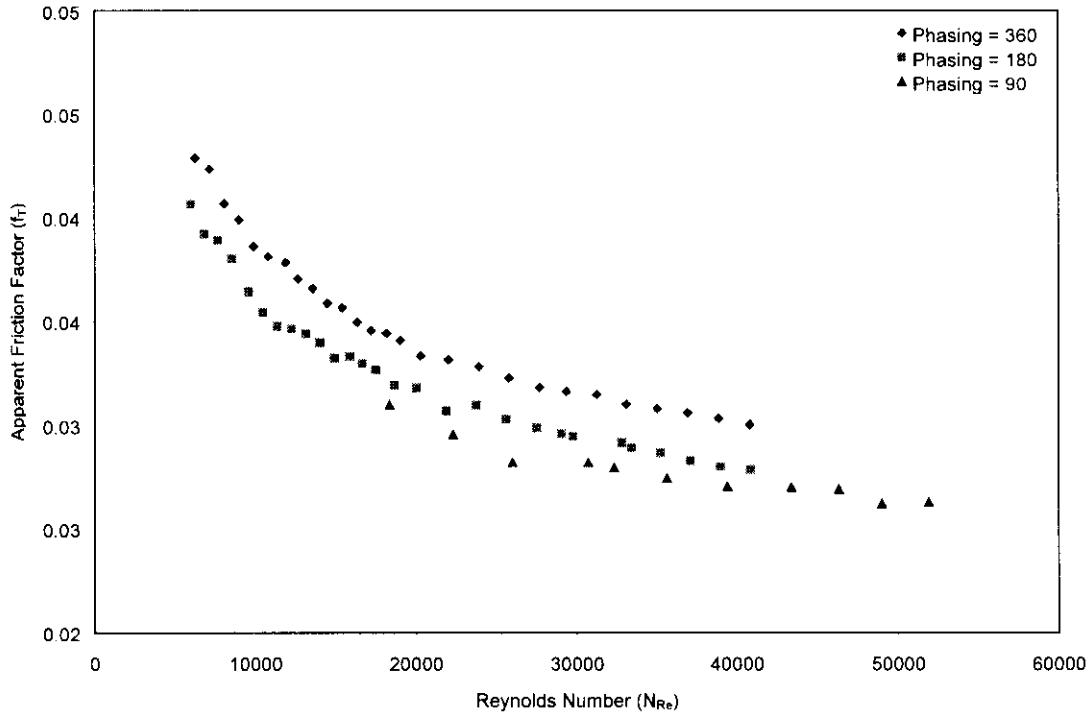

Figure 5-6: Comparison of Experimental Data for Three Phasings (φ = 4.5 slots/ft, ratio = 1/200)

The friction factor is smallest when the phasing is 90°. Since the interaction between the influx and main flow is so complex and few if any analytical studies about it can be found in the literature, the reasons why the completion phasing has such significant effects upon flow behavior in horizontal wells are not clear. The possible reasons can be: 1). When the phasing is smaller, say 90°, the influx can be considered entering from all sides, thus there's smaller twist (distortion) against the main stream velocity profile and therefore there's smaller pressure loss due to momentum change. 2). When the influx enters the main flow from more than one direction, a larger area of the boundary layer is lubricated than if the influx is entering from one direction (360°). The lubrication of the influx can lessen the extent of surface roughness introduced due to completion.

It's interesting to point out that when the phasing is small (90°), both the absolute values of a and b are greater than those when the phasing is 180° or 360°. It means the wall friction factor is larger for small phasing at lower Reynolds numbers while the opposite is true at higher Reynolds numbers. Graphically it means the f_w vs. N_{Re} curve has the steepest decline when the phasing is 90°(see Figure 5-7). From Figure 5-7 we can also notice that for those cases when the completion phasing is 360° the wall friction factor is almost the same as the value predicted by Blasius formula. It means if all the slot openings are aligned on one side of the horizontal pipe, f_w is little affected especially when the Reynolds number is high.

The effect of slots density upon the pressure drop behavior in horizontal wells in this study is quite straightforward: other completion parameters being equal, the apparent friction factor in general increases with the completion density increases mainly due to the

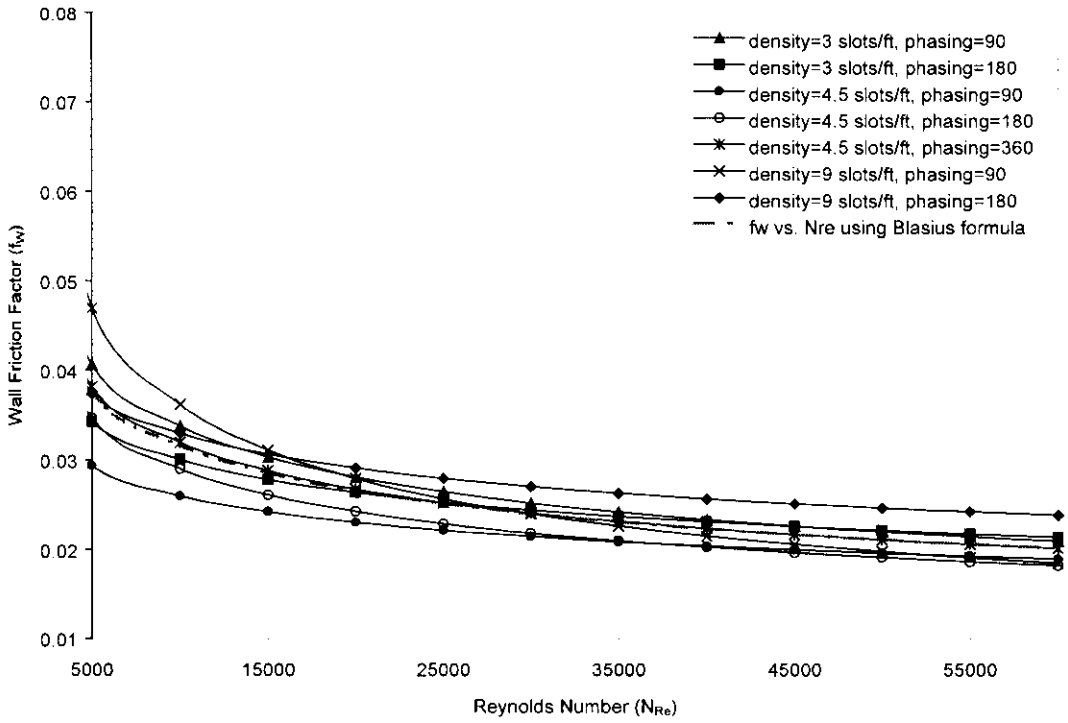

Figure 5-7: f_w vs. N_{Re} for the Multiple Slots Cases (Correlation Prediction)

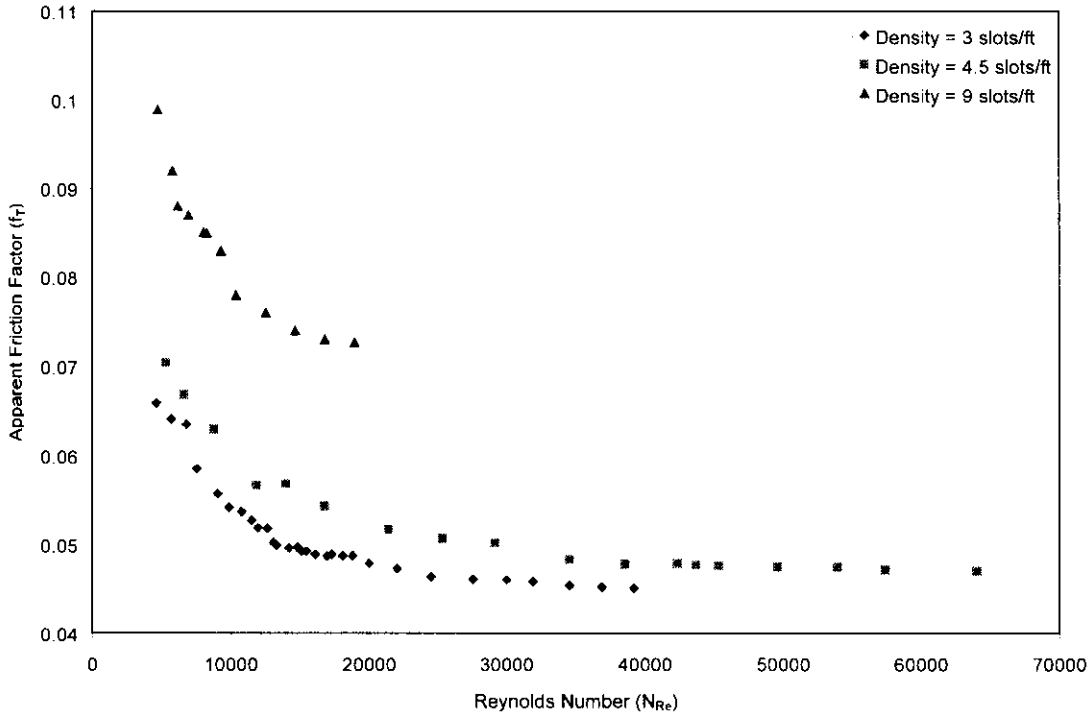

Figure 5-8: Comparison of Experiemntal Data for Three Densities (Phasing = 90 and ratio = 1/50)

increased influx introduced by the extra openings (Figure 5-8). However this may not necessarily be true when the influx over main flow rate ratio is very small, as we will discuss in the multiple perforation section.

5-2. Multiple Perforation Cases

A total of 490 experimental tests are conducted for the six multiple perforation test sections as described in Chapter 3. The tests are conducted with Reynolds numbers ranging approximately from 5,000 to 65,000, influx to main flow rate ratios vary from 1/50 to 1/1000. All the experiments were conducted in room temperature (usually ranging from 75 ^{o}F to 85 ^{o}F). In this section, experiment results for the multiple perforation cases and discussions are presented.

5-2.1 Experiments and Modeling

Figures 5-9 through 5-14 show the variations in apparent friction factor with influx to main flow rate ratios and Reynolds numbers for the six test sections with multiple perforation completions. Each figure is plotted as apparent friction factor f_T vs. Reynolds number N_{Re}, and different data series represent experimental results at different influx to main flow rate ratios. As we can see from the figures, in all the cases the f_T is greater than the smooth pipe friction factor and friction factor from Blasius formula for all the influx to main flow rate ratios (no lubrication effects were observed). In all the cases, the f_T decreases considerably with the decreasing of influx to main flow rate ratio, especially at high flow rate ratio cases. However the decrease of the friction factor is negligible at very low influx over main flow rate ratios.

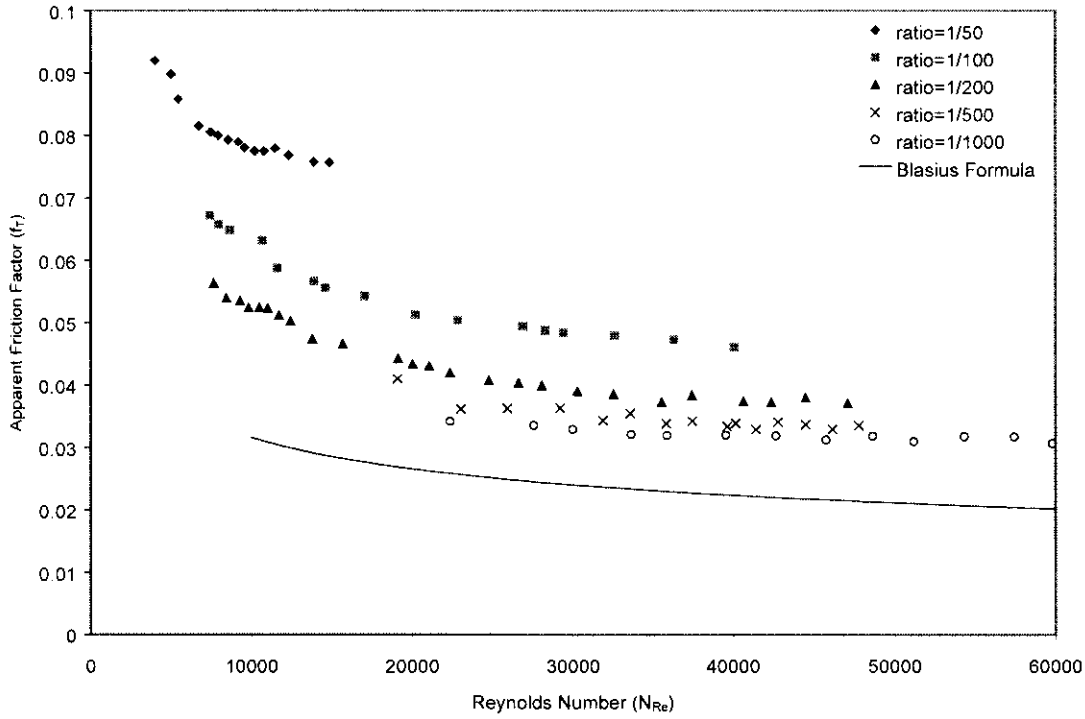

Fig. 5-9: Experimental Data for Test Section 5 (Perforations, 5 shots/ft with 180° phasing)

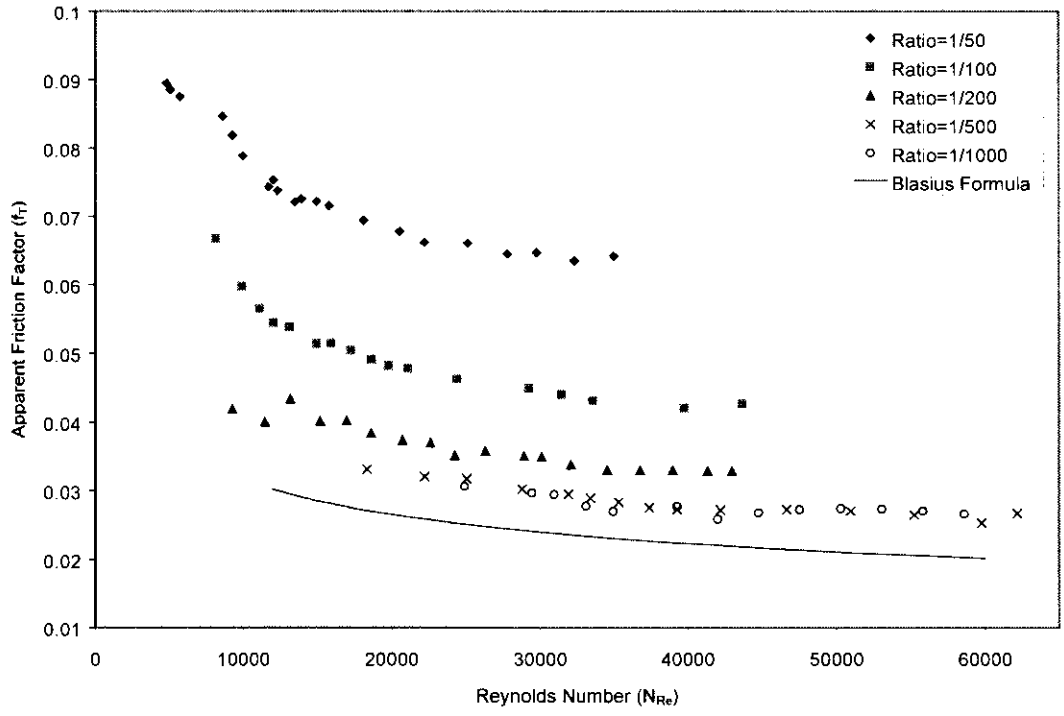

Fig. 5-10: Experimental Data for Test Section 6 (Perforations, 5 shots/ft with 90° phasing)

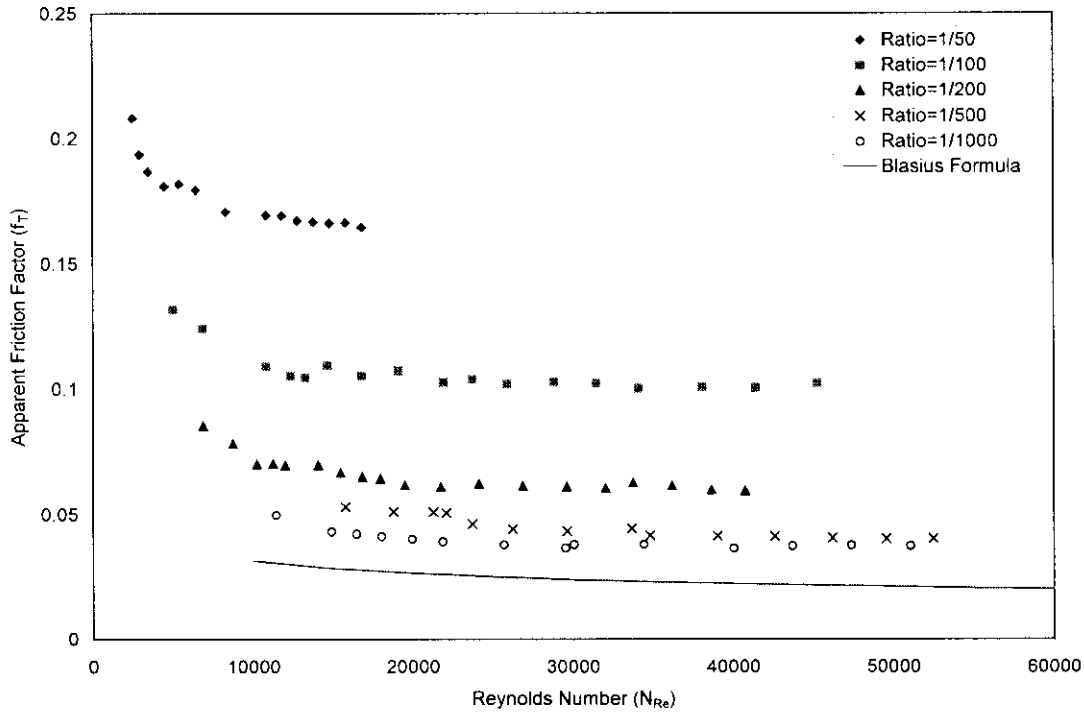

Fig. 5-11: Experimental Data for Test Section 7 (Perforations, 10 shots/ft with 360° phasing)

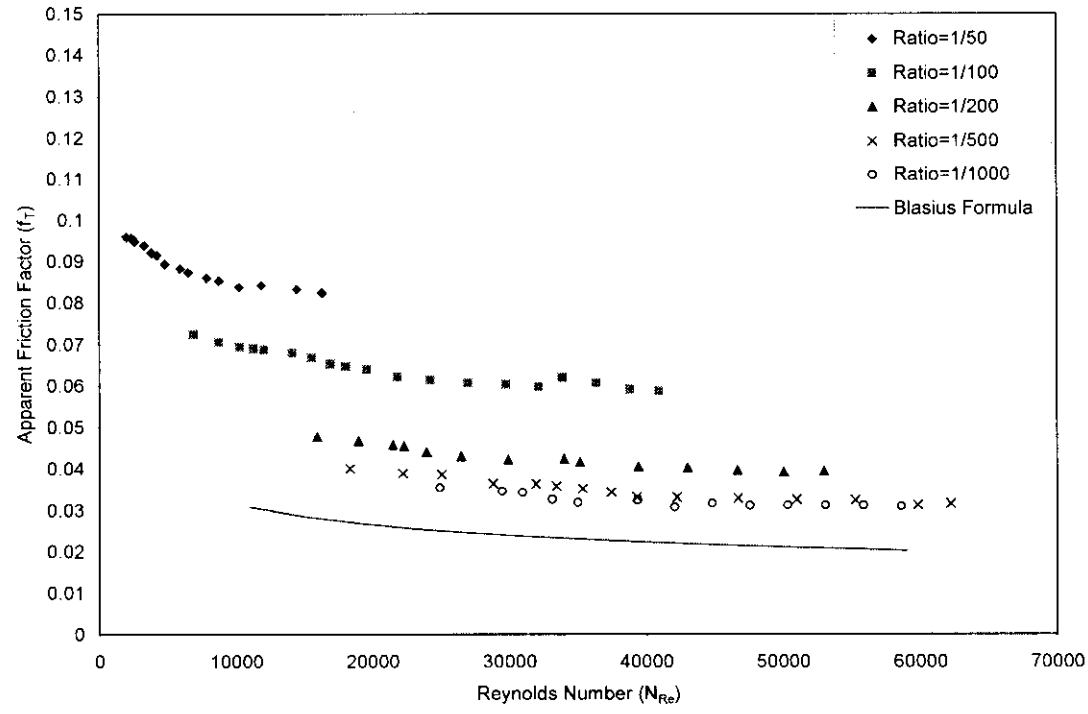

Fig. 5-12: Experimental Data for Test Section 8 (Perforations, 10 shots/ft with 90° phasing)

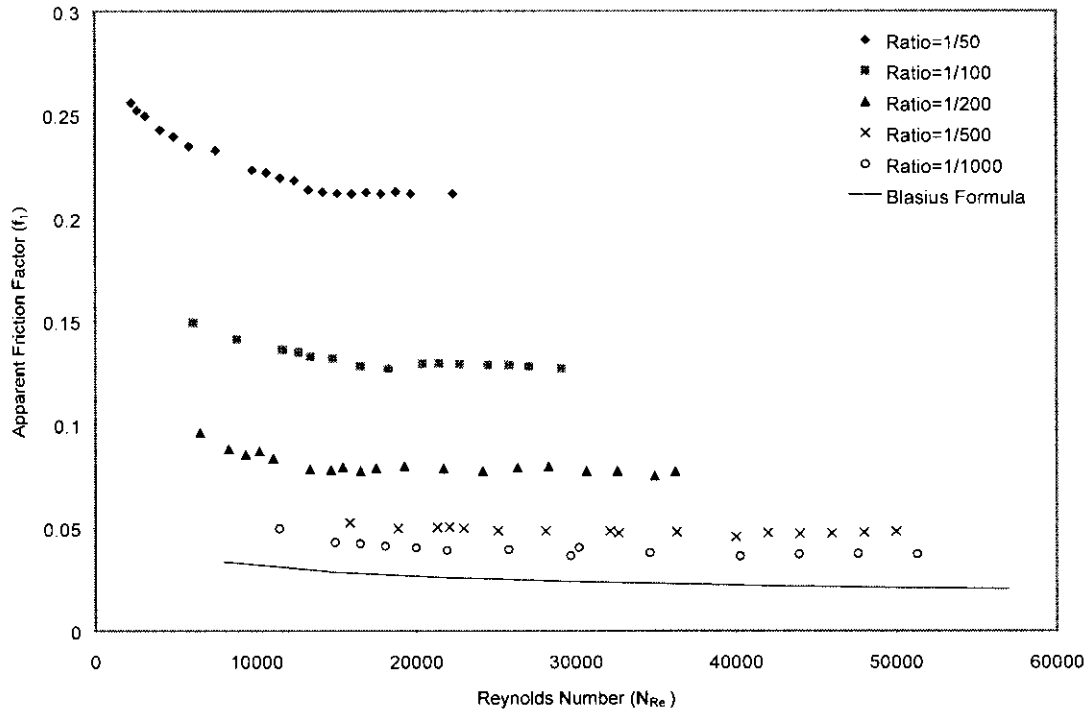

Fig. 5-13: Experimental Data for Test Section 9 (Perforations, 20 shots/ft with 360° phasing)

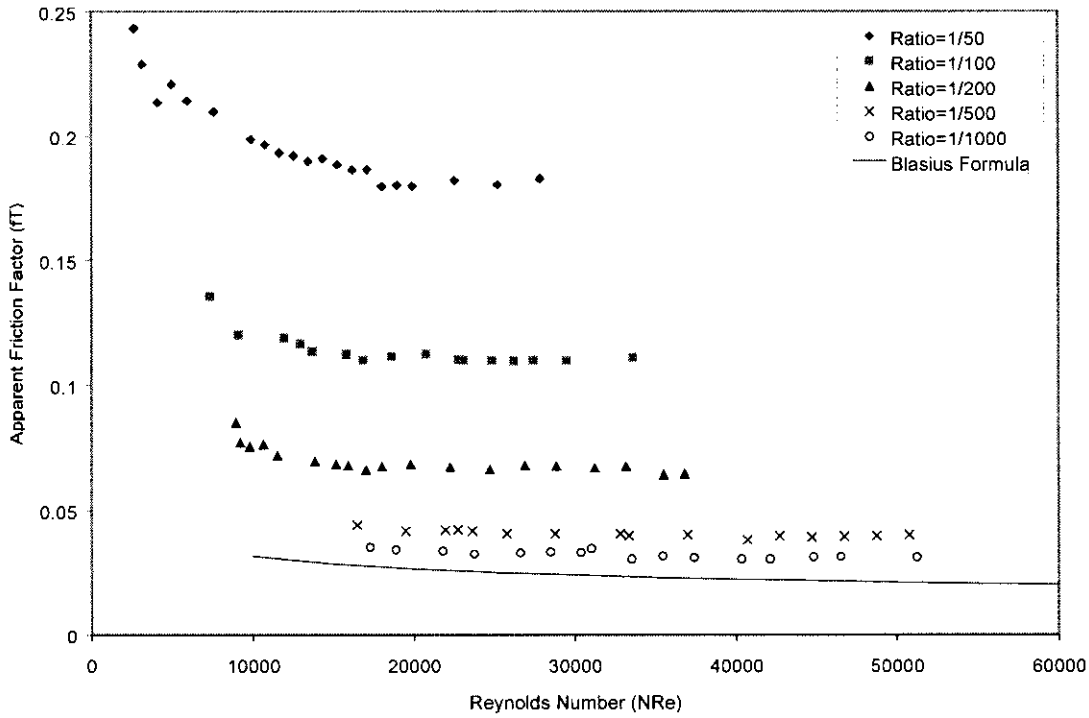

Fig. 5-14: Experimental Data for Test Section 10 (Perforations, 20 shots/ft with 180° phasing)

The data analysis procedure for perforated horizontal wells is the same as that in the multiple slot cases.

The following table lists all the a, b and C_n for all the 9 test sections with multiple perforated openings including the three test sections investigated by Yuan. The data can be directly read to calculate the total friction factor when the completion parameters are the same as or close to those in this study.

Table 5-2: a, b and C_n for the 9 Multiple Perforation Cases

	φ (slots/ft)	α	a	b	C_n
1	5	90	0.87288	-0.340629	2.344056
2	5	180	0.621871	-0.28696	2.02834
3	5	360	0.641	-0.312	2.16852
4	10	90	0.159944	-0.155335	1.489782
5	10	180	0.28711	-0.24584	2.28063
6	10	360	0.755325	-0.308274	3.900876
7	20	90	1.07608	-0.34571	2.693373
8	20	180	4.53217	-0.505271	2.332053
9	20	360	1.07802	-0.345965	2.693826

As we can see from the Table 5-2, both a, b and C_n are rougly in the same numerical ranges as those of the multiple slots cases. For multiple perforation cases, a is in the range of 0.2–3.6, b is in the range of -0.18 – -0.46 and C_n is in the range of 1.4 –

3.9. The following three equations are obtained through regression analysis to estimate a, b and C_n:

$$a = 0.24163 + 0.00275189\varphi^{1.9} + \frac{808.542e^{-\varphi+2.33}}{\alpha} \tag{5-10}$$

$$b = -0.25 + 0.0334316\varphi - 000179399\varphi^{2} - 0.447302\varphi^{0.5} + \frac{0.0513603e^{-\varphi}}{\varphi \cdot \alpha} \tag{5-11}$$

$$C_n = 1.24243 + 0.00467386\alpha + \frac{0.556613 \cdot \varphi^{0.235} \cdot e^{\frac{\alpha}{90}+4.9081}}{\varphi \cdot \alpha} \tag{5-12}$$

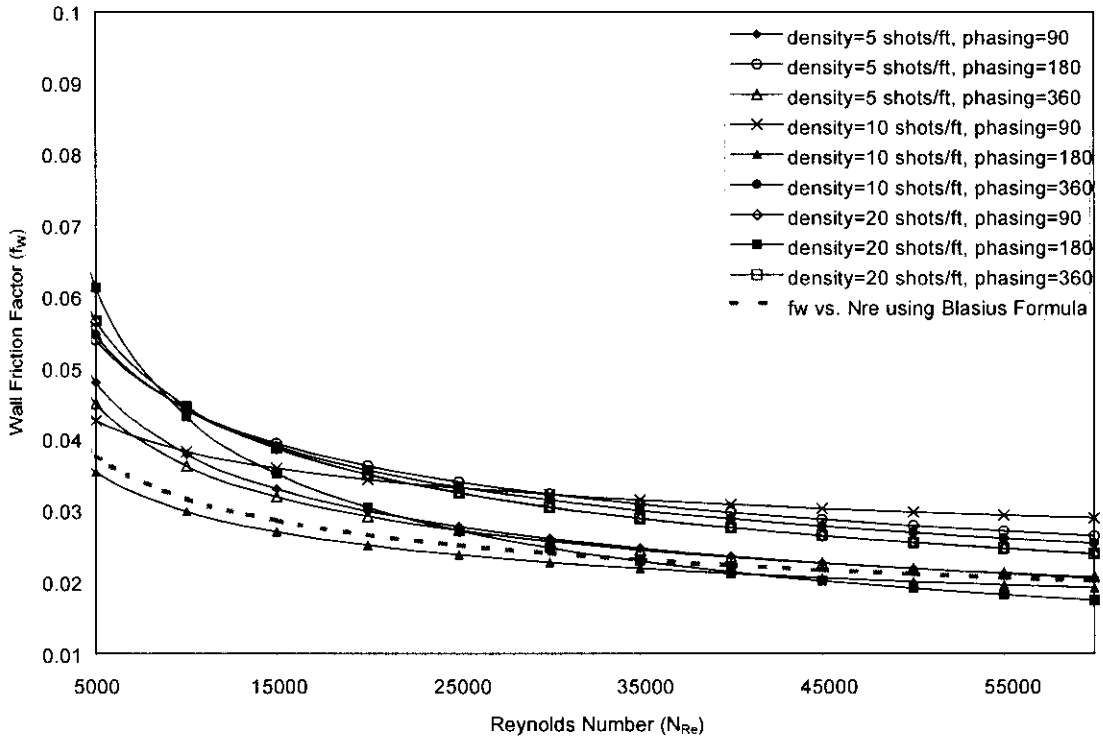

Figure 5-15: f_w vs. N_{Re} for the Multiple Perforation Cases (Correlation Prediction)

It's observed that at high N_{Re} and high influx over main flow rate ratios we can approximate f_w with $0.3156N_{Re}^{-0.25}+0.003$ (See Figure 5-15). Although this approximation introduces up to 20% error in the calculation of f_w, the error in the

calculation of f_T is insignificant since the f_w contribution is much smaller than the influx contribution under those condtions.

5-2.2. Discussions of Effects of Perforation Phasing and Density upon the Pressure Drop Behavior

As mentioned early in the multiple slots section, the completion phasing has significant effect upon the pressure drop behavior in horizontal wells completed with multiple slotted liners. The apparent friction factor usually drops as the phasing decreases when the other parameters being held equal. The same thing is true in multiple perforation cases (See Figures 5-16 and 5-17). What should be pointed out here is the effect of phasing is insignificant once the completion density or the influx over main flow rate ratio becomes too small. Under very small perforation density situations (the distance between two neighboring openings is greater than 8 times of the pipe diameter), the single perforation modeling from Yuan's study should be used to analyze the flow behavior in horizontal wells.

Experimental data are compared for the three perforation densities when the influx to average main flow rate ratios equal to 1/50 and 1/1000 (Figure 5-18 and Figure 5-19). Figure 5-18 shows that for influx to main flow rate ratio equal to 1/50, f_T is higher for the higher perforation density case. Figure 5-19 shows that for influx to main flow rate ratio equal 1/1000, f_T for the three perforation densities are almost the same at low Reynolds number region while f_T is slightly smaller when the density is 20 shots/ft. As discussed in Yuan's study, at very small influx/main flow rate ratios, f_T usually is lower for high perforation density case. One probable reason for this is that the third term on the

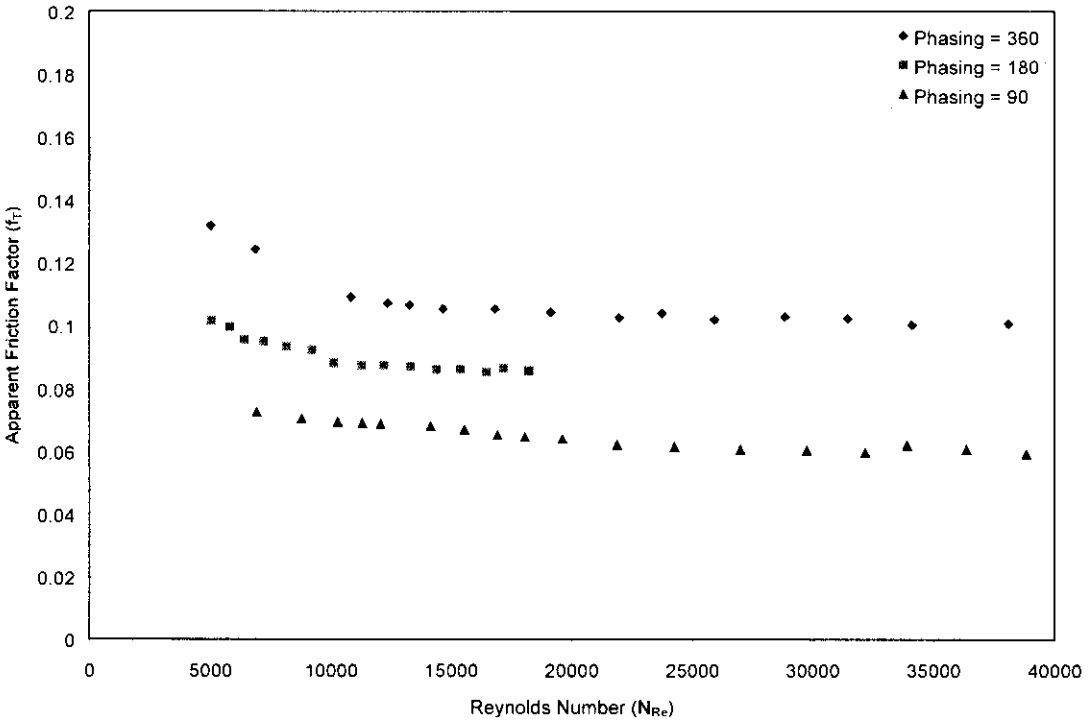

Figure 5-16: Comparison of Experimental Data for Three Phasings (φ = 10 Shots/ft, ratio = 1/100)

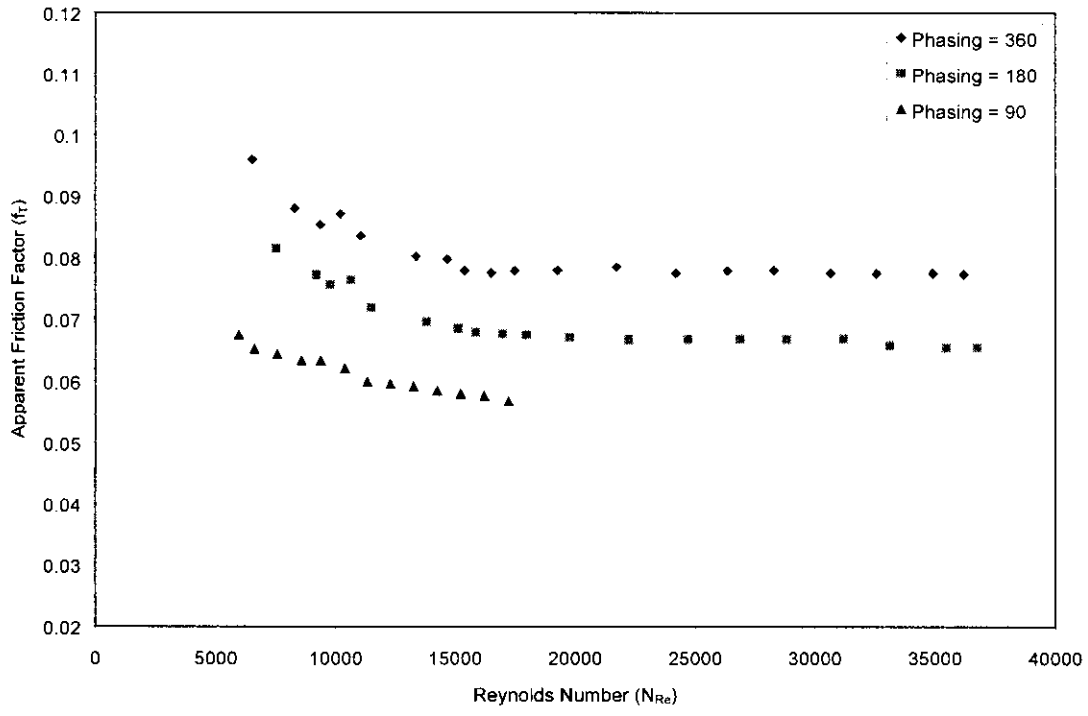

Figure 5-17: Comparison of Experimental Data for Three Phasings (φ =20 Shots/ft, ratio = 1/200)

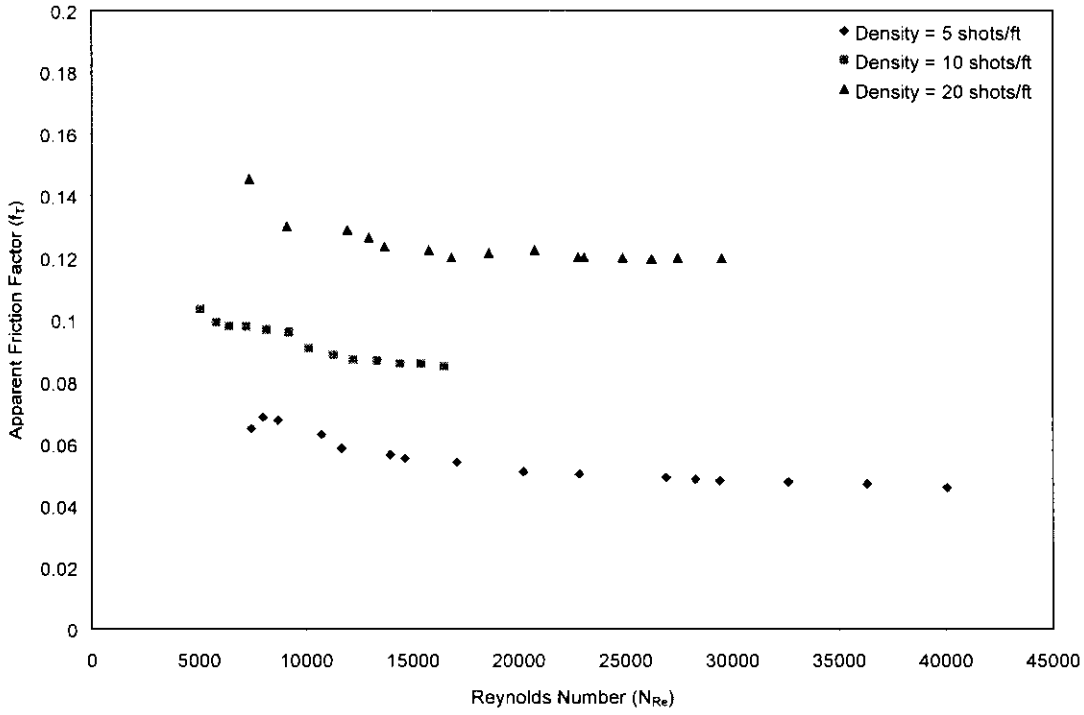

Figure 5-18: Comparison of Experimental Data for Three Densities (α =180°, ratio = 1/100)

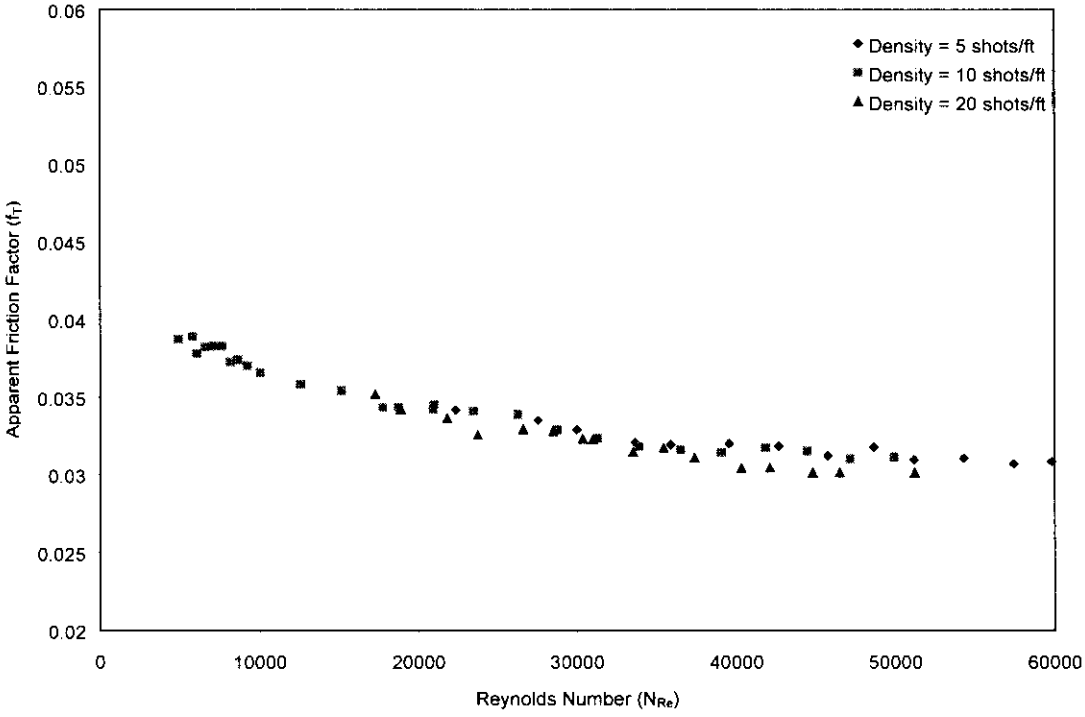

Figure 5-19: Comparison of Experimental Data for Three Densities (α =180°, ratio = 1/1000)

right hand side of Eq. (4-16) (influx contribution to total apparent friction factor) is the dominant term at high influx to main flow rate ratios, while the first term(wall friction factor) is the dominant term at low influx to main flow rate ratios.

5-3: Evaluation of the Correlations

The new apparent friction factor correlation for the multiple perforation cases was first evaluated together with the Asheim *et al.* model against the experimental data obtained in this study.

Figures 5-20 and 5-21 give comparisons of total friction factor predictions for the two correlations and the Blasius formula for smooth pipe. The experimental data from test section 6 are also included with influx over main flow rate ratios of 1/50 and 1/1000. From the comparisons, it is apparent that using different wellbore flow models results in different apparent friction factor predictions at high influx over main flow rate ratios. At low flow influx over main flow rate ratios, the different models yield close results. It should be pointed out that no consideration was given to the perforation distribution in the wellbore flow modeling of the Asheim *et al.* model. The Asheim *et al.* model overpredicts when the influx to main flow rate ratio is high. This is consistent with Yuan's observations when the Asheim *et al.* model was compared with the single perforation correlation.

Next the model derived in this study is compared with Ouyang *et al.* model. Figures 5-22 and 5-23 show comparisons of the wall friction factor predictions for the two models. The wall friction factor is plotted against the local Reynolds number (N_{Re})

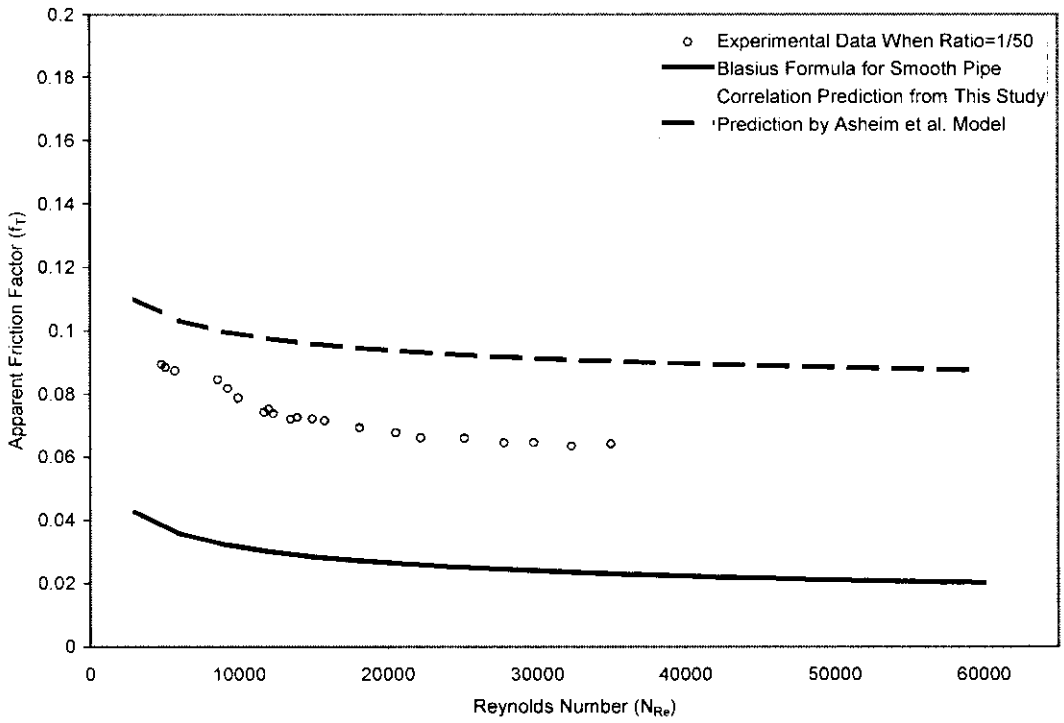

Figure 5-20: Comparison of Different Correlation Predictions
(Perforations, 5 shots/ft, 90° phasing, ratio = 1/50)

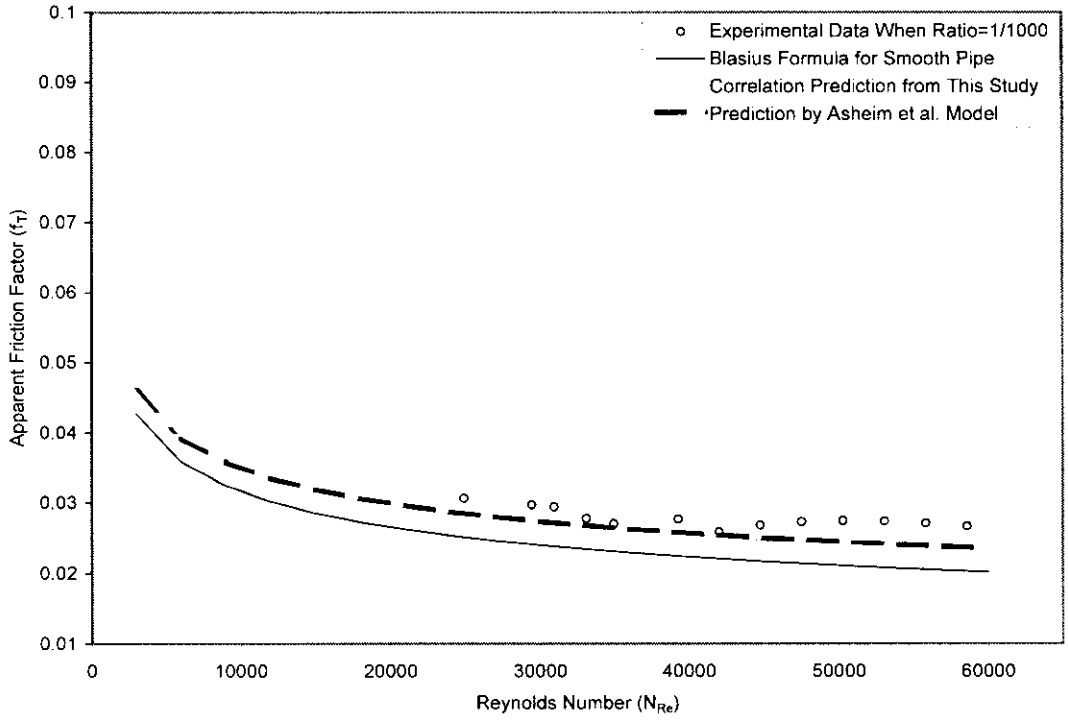

Figure 5-21: Comparison of Different Correlation Predictions
(Perforations, 5 shots/ft, 90° phasing, ratio = 1/1000)

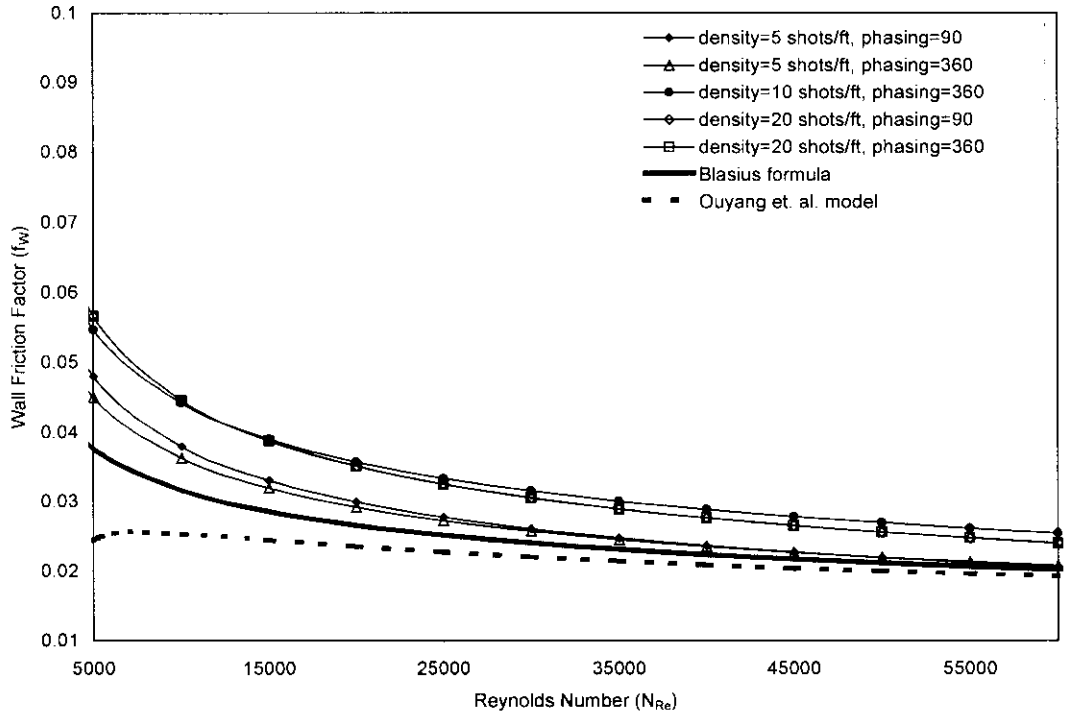

Figure 5-22: f_w vs. N_{Re} for Different Models

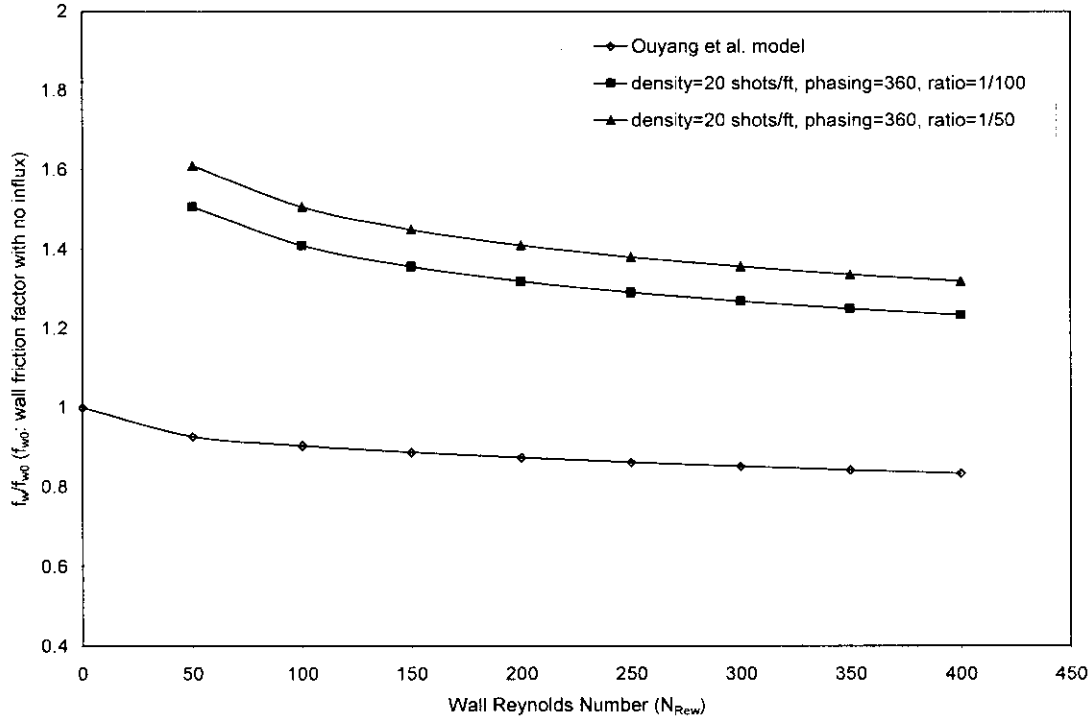

Figure 5-23: f_w/f_{w0} vs. N_{Rew} for Different Models

and the wall Reynolds number (N_{Rew}). In Ouyang's study, it was found that the friction factor was dependent only on the wall Reynolds number and the local Reynolds number. The following two observations were made in their study. First, the inflow from the perforations reduces the wall friction for turbulent flow. Thus the wall friction factor with influx is always smaller than no-influx wall friction factor. Secondly the wall friction factor increases with the local Reynolds number provided that the wall Reynolds number remains constant. Experimental data from this study suggest that the relationship between the wall friction factor and the perforation parameters and flow conditions is more complicated. From the two figures, it can be seen that the wall friction factor is affected by the perforation density, perforation phasing and influx over main flow rate ratio. New study needs to be done to thoroughly investigate the effects of completion geometries upon the wall friction factor.

Figure 5-24 shows the performance of the model derived in this study against large diameter pipe experimental data (Ouyang *et al.* 1995). For simplicity purpose, we used averaged fluid properties in the calculation of pressure drop. As it is evident from the figure, even though the model is derived from experimental data using small diameter pipes, the predictions are matching the experimental data quite well for larger diameter horizontal wells.

The new correlations can be used with confidence for operating conditions dynamically similar to those of the experiments done in this study. The performance of the correlation needs to be tested against field data.

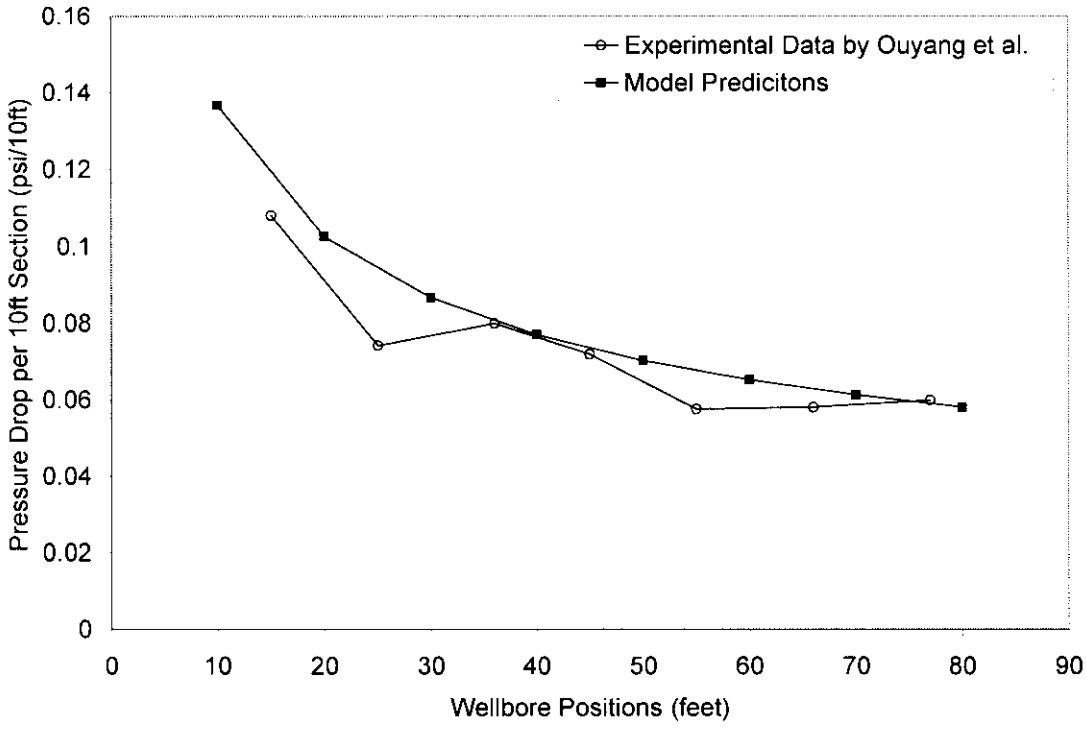

Figure 5-24: Comparisons of Correlation Predictions and Experimental Data

Since the correlations obtained in this study are for multiple opening cases and the completion density and phasing are carefully chosen to ensure that the main flow velocity profile will not fully recover at the next adjacent opening, the correlations may not be used when the completion density is very low. When the perforation density is very low, that is, the distance between two adjacent openings is eight times greater than the pipe diameter, the single injection point correlation proposed by Yuan can be used because the flow will be fully developed before reaching the next injection point. This should be valid except for extremely large influx to main flow rate ratios. Regular pipe friction factor correlations can be used for the fully developed flow region.

When the perforation/slots density is higher, i.e., the distance between two adjacent openings is less than eight pipe diameter, the main flow can not recover from

previous influx disturbances and reach a fully developed flow before reaching the next injection point. Then the correlations derived in this study can be used to estimate the pressure drops.

5-4. Parameters Affecting Apparent Friction Factor

The apparent friction factor correlation was presented in terms of dimensionless parameters, which are functions of some independent variables. Each is discussed below.

1. q_{in}/Q, influx to main flow rate ratio. This dimensionless variable is composed of two dimensionless variables, V_{in}/V and A_p/A. For the same q_{in}/Q, a decrease in V_{in}/V indicates an increase in A_p/A. The influx to main flow rate ratio contributes significantly to apparent friction factor. Each term in Eq. (4-14) is either explicitly or implicitly a function of the influx to main flow rate ratio. For the no fluid injection case, Eq. (4-14) has only two terms on the right hand side, which represent the wall friction and the distortion of the velocity profile. If the flow is fully developed, the velocity distortion term disappears, and the equation is identical to the regular friction factor correlation. f_w is a function of influx to main flow rate ratio as well as Reynolds number, completion density, completion phasing and pipe roughness for the case of fluid injection. Therefore, a regular friction factor correlation cannot be used for the fluid injection case. For large influx to main flow rate ratios, the last two terms in Eq. (4-14) become large mainly due to changes in the velocity field.

2. V_{in}/V, the ratio of the axial velocity component of the injected flow and the main flow velocity. This is an indication of the axial momentum carried to the main flow by the injected fluid. This ratio will affect the C_n value in Eq. (4-16) directly.

3. N_{Re}, the Reynolds number. This is the ratio of inertia forces to viscous forces. N_{Re} will mainly affect the f_w term in Eq. (4-16).

4. n, the number of injection openings. This will affect the last term in Eq. (4-16) directly and will also effect the velocity profiles, that is the β value, therefore affecting other terms in Eq. (4-16) indirectly.

5. α, the phasing of the injection openings. This will influence the velocity distribution, that is the β value, and therefore the f_T.

6. CONCLUSIONS AND RECOMMENDATION

6-1. Conclusions

Based on the work presented in this thesis, the following conclusions have been reached:

1. Ten new test sections were designed and constructed to enable data acquisition at various conditions.

2. The flow behavior in horizontal wells for two completion geometries, slotted pipe and perforated pipe, was investigated and for each completion geometry, various perforation or slot densities and distribution patterns were investigated.

3. A large amount of experimental data was acquired with fluid injection case. The influx to main flow rate ratios investigated range from 1/50 to 1/1000. The Reynolds numbers range approximately from 5,000 to 65,000.

4. A general expression for apparent friction factor has been developed from momentum equation and continuity equation considerations. New simple correlations for apparent friction factor have been developed by applying experimental data to the general expression for apparent friction factor.

6. In general fluid influx will increase the apparent friction factor along the horizontal wellbore, but in some cases the influx will decrease the apparent friction factor which means that the injected fluid has a lubrication effect. Lubrication effect typically can only be found when the completion density is not too high, the completion phasing is small and the influx/main flow rate ratio is small.

7. For horizontal wells completed with slotted liners, for the same slot number, the apparent friction factor is smaller when the slot phasing is lower. For perforated horizontal wells the same observation holds for large perforation density. At small perforation densities, for the same perforation number, we found the apparent friction factor is higher for higher phasing.

8. Other parameters being equal, apparent friction factor usually increases with the increase of completion density at high injection rate. At low injection rate, for the perforation case, the apparent friction factor is slightly larger for smaller perforation density.

6-2. Recommendations

The following are recommended for future studies:

1. Conduct experiments for multiple injection points at completion densities and completion patterns other than those discussed in this study. Additional data will improve the accuracy of friction factor correlation prediction.

2. Measure the velocity profile along the flow-developing region to obtain insight into the interaction between influx and main flow and between influxes.

3. Test the model against field data that will involve much larger Reynolds numbers than those included in laboratory studies once those data become available.

4. More robust computer programs are needed in the data analysis procedure. Typical curve fitting software packages usually give large errors in multiple-variable regression analysis.

5. Conduct experiments for single-phase flow of gases.

6. Build a large-scale test facility and conduct experiments for larger Reynolds numbers and for multiphase flow conditions.

7. NOMENCLATURE

Symbol	Description
A	pipe cross sectional area (m^2)
C_n	coefficient as defined by Eq. (4-15) (-)
d	pipe diameter (m)
f^o	regular pipe friction factor (Moody) (-)
f_T	apparent friction factor (Moody) (-)
f_w	wall friction factor (Moody) (-)
J_r	specific productivity index (m^2/pa.s)
L	pipe length (m)
L_d	flow developing length (m)
N_{Re}	Reynolds number (-)
p	pressure(pa)
p_w	well pressure (pa)
Q	main flow rate (m^2/s)
q_{in}	volumetric influx flow rate from each injection opening (m^2/s)
q_r	specific inflow into the well (m^2/s)
q_w	cumulative flow rate (m^3/s)
R	pipe radius (m)
T	temperature (^oC)

$\bar{u}$	average main flow velocity (m/s)
V_p	average influx velocity from each injection opening (m/s)
V_x, V_r	velocity component as shown in Fig. 4-1 (m/s)
ΔX	distance between two adjacent perforations/slots (m)
Δx	a distance as shown in Fig. 4-1 (m)
x	distance along a horizontal well (m)

Symbol (Greeks)	Description
α	completion phasing (-)
β	momentum correction factor (-)
ε	absolute pipe roughness (m)
ϕ	defined by Eq. (4-12)
φ	the density of injection openings defined by Eq. (4-13) (1/m)
μ	dynamic viscosity (Ns/m^2)
υ	kinematic viscosity (m^2/s)
ρ	density (kg/m^3)
τ_w	wall shear stress (N/m^2)

Subscript	Description
1	variables pertinent to cross section 1-1
2	variables pertinent to cross section 2-2
i	variables pertinent to initial value
in	variables pertinent to influx stream
p	variables pertinent to perforation

r	variables pertinent to radial direction
w	variables pertinent to wall or well
x	variables pertinent to axial direction
t	variables pertinent to turbulent

8. REFERENCES

1. Asheim, H., Kolnes, J., and Oudeman, P.: "A Flow Resistance Correlation for Completed Wellbore," Journal of Petroleum Science and Engineering, 8 (1992), pp. 97-104.

2. Brekke, K.: "New and Simple Completion Methods for Horizontal Wells Improve the Production Performance in High Permeability, Thin Oil Zones," paper SPE 24762, presented at SPE 67th Annual Technical Conference and Exhibition, Washington, D.C., Oct. 4-7, 1992.

3. Beggs, H. D., and Brill, J. P., "Two Phase Flow in Pipes", 1998.

4. Bird, R., Stewart, W., Lightfoot, E., "Transport Phenomena", John Wiley and Sons, 1993 Edition.

5. Brekke, K., Johansen, T. E., and Olufsen, R.: "A New Modular Approach to Comprehensive Simulation of Horizontal Wells," paper SPE 26518, presented at SPE 68th Annual Technical Conference and Exhibition, Houston, Texas, Oct. 3-6, 1993.

6. Brice, B. W.: "Production Impacts on ΔP Friction in Horizontal Production Wells," paper SPE 23666, presented at SPE Second Latin American Petroleum Engineers Conference, II LAPEC, Caracas, Venezuela, March 8-11, 1992.

7. Denn, M. M.: "Process Fluid Mechanics," Prentice-Hall, Inc., 1980

8. Dikken, B. J.: "Pressure Drop in Horizontal Wells and its Effect on Their Production Performance," paper SPE 19824, presented at SPE 64th Annual Technical Conference and Exhibition, San Antonio, TX, Oct. 8-11, 1989.

9. Hornbeck, R. W., Rouleau, W. T., and Osterle, F.: " Laminar Entry Problem in Porous Tubes," The Physics of Fluids, vol. 6, number 11, November 1963, pp.1649-1654.

10. Ihara, M.: "Two-Phase Flow in Horizontal Wellbores," M. S. Thesis, The University of Tulsa, 1991.

11. Joshi, S. D.: "Horizontal Well Technology," Pennwell Publishing Co., 1991.

12. Kato, H., Fujii, Y., Yamaguchi, H. and Miyanaga, M.: "Frictional Drag Reduction by Injecting High-Viscosity Fluid into Turbulent Boundary Layer," Journal of Fluids Engineering, June 1993, vol. 115, pp. 207-212.

13. Kinney, R. B.: "Fully Developed Frictional and Heat-transfer Characteristics of Laminar Flow in Porous Tubes," Int. J. Heat Mass Transfer, vol. 11, 1968, pp.1393-1401.

14. Kloster, J.: "Experimental Research on Flow Resistance in Perforated Pipe," M.S Thesis, Norwegian Institute of Technology, 1990.

15. Norris, S. O., Hunt, J. L., and Soliman, M. Y.: "Predicting Horizontal Well Performance: A Review of Current Technology," paper SPE 21793, presented at the Western Regional Meeting held in Long Beach, California, March 20-22, 1991.

16. Novy, R. A.: "Pressure Drops in Horizontal Wells: When Can They Be Ignored?," paper SPE 24941, presented at SPE 67th Annual Technical Conference and Exhibition, Washington, D.C., Oct. 4-7, 1992.

17. Olson, R. M. and Eckert, E. R. G.: "Experimental Studies of Turbulent Flow in a Porous Circular Tube with Uniform Fluid Injection Through the Tube Wall," Journal of Applied Mechanics, March 1966, pp. 7-17.

18. Ouyang, L., Arbabi, S. and Aziz, K.: "General Wellbore Flow Model for Horizontal, Vertical, and Slanted Well Completions," SPE 36608, presented at 1996 SPE Annual Technical Conference and Exhibition, Denver, Colorado, Oct. 6-9, 1996.

19. Ouyang, L.,Petalas N., Schroeder D., Arbabi, S. and Aziz, K.: "An Experimental Study of Single-Phase and Two-Phase Fluid Flow in Horizontal Wells," SPE 46221, presented at 1998 SPE Western Regional Meeting, Bakersfield, California, May 10-13, 1998.

20. Ozkan, E, Sarica, C., Haciislamoglu, M. and Raghavan, R.: "The Influence of Pressure Drop Along the Wellbore on Horizontal Well Productivity," paper SPE 25502, presented at SPE 1993 Production Operations Symposium, Oklahoma City, OK, March 21-23, 1993.

21. Schulkes, R.: "Modeling Flow Characteristics in a Horizontal Wall," Presented at Fluent 1996 European Users' Group Meeting, May 20-21, 1996.

22. Shapiro, A. H., Siegel, R. and Kline, S. J.: "Friction Factor in the Laminar Entry Region of a Smooth Tube, " Proc. Second U. S. National Congress of Appl. Mech., June 1954, pp. 733-741.

23. Shikari, Y. A. and Bergin, S. R.: "Horizontal Well Increases Gas Storage Well Deliverability," Oil and Gas Journal, Feb. 22, 1993, pp. 63.

24. Streeter, V. L. and Wylie, E. B.: "Fluid Mechanics," McGraw-Hill Book Company, Seventh Edition.

25. Su, Z. and Gudmundsson, J. S.: "Pressure Drop in Perforated Pipes: Experiments and Analysis," paper SPE 28800, presented at the SPE Asia Pacific Oil & Gas Conference, Melbourne, Auatralia, Nov. 7-10, 1994.

26. Yuan, H.: "Investigation of Single Phase Liquid Flow Behavior in a Single Perforation Horizontal Well," M.S. Thesis, The University of Tulsa, 1994.

27. Yuan, H.: "Investigation of Single Phase Liquid Flow Behavior in Horizontal Wells," Ph.D Dissertation, The University of Tulsa, 1997.

28. Yuan, H., Sarica, C. and Brill, J. P.: "Effect of Perforation Density on Single Phase Liquid Flow Behavior in Horizontal Wells," SPE 37109, presented at the 1996 International Conference on Horizontal Well Technology, Calgary, Alberta, Canada, November 18-20, 1996.

29. Yuan, H., Sarica, C., Miska, S. and Brill, J. P.: "An Experimental and Analytical Study of Single Phase Liquid Flow in a Horizontal Well," published in ASME Journal of Energy Resources Technology, Vol. 119, March 1997, pp. 20-25.

30. Yuan, S. W. and Finkelstein, A. B.: "Laminar Pipe Flow With Injection and Suction Through a Porous Wall," Trans. ASME, vol. 78, 1956, pp. 719-724.

APPENDIX: EXPERIMENTAL DATA

Table A-1: Experimental Data for Test Section 1 (Slots, $\alpha = 90^{\circ}$, $\varphi = 4.5$ slots/ft)

N_{Re}	q_{in}/Q	f_T	N_{Re}	q_{in}/Q	f_T	N_{Re}	q_{in}/Q	f_T	N_{Re}	q_{in}/Q	f_T	N_{Re}	q_{in}/Q	f_T
5318.90	0.02	0.070387	11592.64	0.01	0.038141	11374.50	0.005	0.032161	11774.94	0.002	0.031878	38159.17	0.001	0.020607
6595.33	0.02	0.066833	15225.13	0.01	0.034550	13680.99	0.005	0.031946	12993.50	0.002	0.030828	41041.96	0.001	0.020540
8759.87	0.02	0.062958	19356.40	0.01	0.035079	18350.27	0.005	0.030994	14855.51	0.002	0.029116	42776.90	0.001	0.020569
11828.78	0.02	0.056680	22872.51	0.01	0.033539	22300.55	0.005	0.029552	17124.46	0.002	0.026716	44902.08	0.001	0.020343
13967.98	0.02	0.056825	27273.30	0.01	0.033402	26008.38	0.005	0.028227	19787.44	0.002	0.026902	48052.23	0.001	0.020316
16784.28	0.02	0.054296	32965.93	0.01	0.032658	30717.54	0.005	0.028226	21959.15	0.002	0.025486	50103.44	0.001	0.019952
21414.10	0.02	0.051676	39846.19	0.01	0.031711	32332.55	0.005	0.027957	24143.65	0.002	0.025041	52168.43	0.001	0.020018
25343.31	0.02	0.050670	46108.03	0.01	0.031047	35621.30	0.005	0.027454	26777.08	0.002	0.024656	54186.13	0.001	0.019842
29152.51	0.02	0.050143	49081.36	0.01	0.030865	39405.72	0.005	0.027054	29145.63	0.002	0.024410	54340.14	0.001	0.019939
34549.93	0.02	0.048278	53345.69	0.01	0.030565	43390.78	0.005	0.026993	31508.25	0.002	0.024550	57274.09	0.001	0.019903
38570.73	0.02	0.047786	58957.99	0.01	0.030418	46325.42	0.005	0.026901	35437.37	0.002	0.023570			
43695.44	0.02	0.047697	65984.55	0.01	0.030208	49000.12	0.005	0.026214	37393.97	0.002	0.023697			
42340.09	0.02	0.047845	68729.89	0.01	0.030126	51913.07	0.005	0.026293	40015.26	0.002	0.023625			
45336.32	0.02	0.047620				54332.00	0.005	0.026023	43861.06	0.002	0.023357			
49595.30	0.02	0.047481				57489.00	0.005	0.026222	46076.00	0.002	0.023218			
53944.72	0.02	0.047453				62123.64	0.005	0.025744	48018.00	0.002	0.023051			
57422.77	0.02	0.047630							50891.90	0.002	0.022625			
64040.29	0.02	0.047113							54599.99	0.002	0.022389			
									56113.56	0.002	0.022515			
									58777.76	0.002	0.022407			

Table A-2: Experimental Data for Test Section 2 (Slots, $\alpha = 180^{o}$, $\varphi = 3$ slots/ft)

N_{Re}	q_{in}/Q	f_T	N_{Re}	q_{in}/Q	f_T	N_{Re}	q_{in}/Q	f_T	N_{Re}	q_{in}/Q	f_T	N_{Re}	q_{in}/Q	f_T
2234.97	0.02	0.068565	4464.35	0.01	0.056167	7385.85	0.005	0.046506	16345.91	0.002	0.04055	33616.4	0.0013	0.034774
2390.02	0.02	0.068993	4735.66	0.01	0.055791	9601.77	0.005	0.045399	21856.43	0.002	0.03956	35149.5	0.0013	0.034652
2661.15	0.02	0.067501	5683.64	0.01	0.054633	11487.35	0.005	0.045345	23026.91	0.002	0.03795	37875.5	0.0013	0.034628
2973.26	0.02	0.065446	6640.52	0.01	0.053675	12162.58	0.005	0.045239	23787.34	0.002	0.03797	38964.8	0.0013	0.034581
3176.16	0.02	0.064451	7387.31	0.01	0.053606	12770.54	0.005	0.045061	25154.22	0.002	0.03783	40237.1	0.0013	0.03458
3848.76	0.02	0.063835	7916.39	0.01	0.053063	12998.35	0.005	0.044969	26320.40	0.002	0.03764	41748.8	0.0013	0.034535
4932.06	0.02	0.062728	8673.26	0.01	0.052962	14983.08	0.005	0.044953	27002.82	0.002	0.03724	42692.3	0.0013	0.034521
5651.39	0.02	0.061048	9841.29	0.01	0.052759	16784.58	0.005	0.043652	29267.73	0.002	0.03686	44330.2	0.0013	0.034532
5799.06	0.02	0.060926	10192.00	0.01	0.051616	19656.81	0.005	0.042750	32944.92	0.002	0.03708	45407.9	0.0013	0.034347
7471.32	0.02	0.059688	11889.33	0.01	0.050560	22058.71	0.005	0.042412	34442.12	0.002	0.03674	46783.7	0.0013	0.034244
8833.01	0.02	0.058441	11566.44	0.01	0.050566	26493.19	0.005	0.041431	36630.31	0.002	0.03671	48727.4	0.0013	0.034145
11170.82	0.02	0.057258	15275.09	0.01	0.049356	27469.99	0.005	0.042070	37883.43	0.002	0.03634	52250.1	0.0013	0.034042
13043.16	0.02	0.057423	18998.34	0.01	0.048321	30112.61	0.005	0.040994	39793.93	0.002	0.03636			
14575.55	0.02	0.054908	21056.98	0.01	0.047323	33116.43	0.005	0.041391	40753.98	0.002	0.03596			
15821.17	0.02	0.054577	23344.12	0.01	0.046905	34002.55	0.005	0.040395	43223.73	0.002	0.03601			
17057.32	0.02	0.053954	25450.00	0.01	0.046026	35456.65	0.005	0.040377	44766.97	0.002	0.03622			
19050.00	0.02	0.053736	28777.62	0.01	0.045978	36617.03	0.005	0.040378	46480.13	0.002	0.03602			
21150.15	0.02	0.053269	32082.31	0.01	0.045574	38200.52	0.005	0.040370	47371.10	0.002	0.03576			
21586.57	0.02	0.052966	34411.80	0.01	0.045325	39784.10	0.005	0.040356	49183.70	0.002	0.03582			
23018.43	0.02	0.052426	36702.90	0.01	0.044840									
25473.05	0.02	0.052399	39297.53	0.01	0.045041									
26769.22	0.02	0.052149												
28466.35	0.02	0.051899												
29486.64	0.02	0.052232												

Table A-3: Experimental Data for Test Section 3 (Slots, $\alpha = 90^{o}$, $\varphi = 3$ slots/ft)

N_{Re}	q_{in}/Q	f_T	N_{Re}	q_{in}/Q	f_T	N_{Re}	q_{in}/Q	f_T	N_{Re}	q_{in}/Q	f_T	N_{Re}	q_{in}/Q	f_T
4616.55	0.02	0.073921	11069.55	0.01	0.050281	12819.04	0.005	0.042596	17779.92	0.002	0.035671	35856.18	0.001	0.031570
5680.87	0.02	0.072132	12952.11	0.01	0.049744	15246.02	0.005	0.041972	19526.91	0.002	0.034168	37840.16	0.001	0.031685
6775.02	0.02	0.071531	14420.32	0.01	0.048349	17915.11	0.005	0.040850	21257.13	0.002	0.034230	38705.23	0.001	0.031816
7528.34	0.02	0.066513	15120.20	0.01	0.047872	19009.70	0.005	0.039912	22020.76	0.002	0.034189	40905.43	0.001	0.030941
9033.75	0.02	0.063705	16376.27	0.01	0.047075	20689.15	0.005	0.039719	24227.03	0.002	0.034286	41968.94	0.001	0.030133
9857.72	0.02	0.062191	17702.22	0.01	0.046964	22778.44	0.005	0.038976	25086.67	0.002	0.034037	43648.19	0.001	0.030812
10749.18	0.02	0.061708	19122.33	0.01	0.046729	24252.74	0.005	0.038432	27213.72	0.002	0.033140	44753.72	0.001	0.030359
11482.06	0.02	0.060722	20772.68	0.01	0.045233	26757.43	0.005	0.038234	29002.76	0.002	0.033086	46643.02	0.001	0.030143
11935.39	0.02	0.059863	21887.84	0.01	0.045901	28545.64	0.005	0.038294	31821.70	0.002	0.033168	47608.44	0.001	0.030445
12635.67	0.02	0.059830	23490.38	0.01	0.044296	31003.08	0.005	0.038173	33884.19	0.002	0.032945	49353.29	0.001	0.030266
13060.49	0.02	0.058210	25043.76	0.01	0.044428	33157.31	0.005	0.038253	36647.56	0.002	0.033149	50763.19	0.001	0.030239
13295.83	0.02	0.057909	27556.01	0.01	0.043294	35070.82	0.005	0.038196	37298.84	0.002	0.032946	52690.73	0.001	0.029796
14176.52	0.02	0.057610	28846.69	0.01	0.043238	36827.29	0.005	0.037897	40306.38	0.002	0.032826			
14804.92	0.02	0.057690	30337.29	0.01	0.043264	37835.22	0.005	0.037843	40796.45	0.002	0.032764			
15072.61	0.02	0.057280	31199.57	0.01	0.043258	39361.29	0.005	0.037844	42175.30	0.002	0.032624			
15430.77	0.02	0.057238	31963.02	0.01	0.043241	39970.15	0.005	0.037944	44141.66	0.002	0.032474			
16081.06	0.02	0.056883	33487.15	0.01	0.042686	40369.43	0.005	0.037762	45249.88	0.002	0.032357			
16936.38	0.02	0.056720	34878.99	0.01	0.042300	40990.12	0.005	0.037808	46878.49	0.002	0.032096			
17303.96	0.02	0.056889	36736.52	0.01	0.042222	42513.39	0.005	0.037544	48209.74	0.002	0.032231			
18068.33	0.02	0.056751	42667.04	0.01	0.042865	45156.32	0.005	0.037635	49667.31	0.002	0.031578			
18802.57	0.02	0.056745							51956.21	0.002	0.031670			
19997.75	0.02	0.055878												
22015.48	0.02	0.055321												
24500.75	0.02	0.054398												
27568.00	0.02	0.054113												
30004.55	0.02	0.054041												
31899.65	0.02	0.053842												
34568.22	0.02	0.053419												
36895.81	0.02	0.053541												

Table A-4: Experimental Data for Test Section 4 (Slots, $\alpha = 180^{o}$, $\varphi = 9$ slots/ft)

N_{Re}	q_{in}/Q	f_T	N_{Re}	q_{in}/Q	f_T	N_{Re}	q_{in}/Q	f_T	N_{Re}	q_{in}/Q	f_T	N_{Re}	q_{in}/Q	f_T
1933.44	0.02	0.109381	5495.97	0.01	0.076332	19385.46	0.005	0.053424	20941.19	0.002	0.039284	26514.18	0.001	0.037101
2706.20	0.02	0.101200	6657.71	0.01	0.075322	20423.20	0.005	0.052855	22656.27	0.002	0.039466	29916.11	0.001	0.036220
3123.31	0.02	0.101000	7987.72	0.01	0.073146	20423.20	0.005	0.052472	24303.04	0.002	0.038448	34290.93	0.001	0.033666
3392.36	0.02	0.100200	8996.21	0.01	0.072575	21886.12	0.005	0.051824	26146.68	0.002	0.038998	35982.06	0.001	0.036135
3726.84	0.02	0.099850	10269.88	0.01	0.072333	22666.93	0.005	0.051259	27541.08	0.002	0.038975	38160.66	0.001	0.034312
4090.39	0.02	0.097640	11093.36	0.01	0.071899	23510.98	0.005	0.050602	30125.69	0.002	0.038329	40278.85	0.001	0.034324
4684.02	0.02	0.096550	15412.65	0.01	0.069736	25433.83	0.005	0.049870	32809.34	0.002	0.038614	42035.10	0.001	0.034134
5740.51	0.02	0.094990	19166.32	0.01	0.068192	27334.37	0.005	0.049586	35339.07	0.002	0.038299	43254.43	0.001	0.033943
6335.49	0.02	0.094000	21406.42	0.01	0.067554	30687.10	0.005	0.050368	37773.14	0.002	0.038183	47007.21	0.001	0.033504
7639.18	0.02	0.093210	23827.99	0.01	0.066586	33641.06	0.005	0.048709	40758.83	0.002	0.038468	50821.67	0.001	0.032578
8499.36	0.02	0.090110	26671.85	0.01	0.064001	37539.21	0.005	0.049388	42915.99	0.002	0.038753	54718.92	0.001	0.031504
9935.99	0.02	0.089720	29515.70	0.01	0.063555	40042.17	0.005	0.048096	44317.07	0.002	0.038038	58348.82	0.001	0.030437
11519.10	0.02	0.089100	32359.55	0.01	0.063218	44073.36	0.005	0.048373						
14051.33	0.02	0.088621	35203.41	0.01	0.062000	47989.53	0.005	0.048108						
15871.99	0.02	0.087564	38047.26	0.01	0.062955									
			38455.00	0.01	0.063000									
			39558.00	0.01	0.062723									
			40225.00	0.01	0.062860									
			40891.11	0.01	0.062166									
			43734.97	0.01	0.062545									
			46578.82	0.01	0.062005									

Table A-5: Experimental Data for Test Section 5 (Perforations, $\alpha = 180^{o}$, $\varphi = 5$ shots/ft)

N_{Re}	q_{in}/Q	f_T	N_{Re}	q_{in}/Q	f_T	N_{Re}	q_{in}/Q	f_T	N_{Re}	q_{in}/Q	f_T	N_{Re}	q_{in}/Q	f_T
4010.18	0.02	0.091954	7419.65	0.01	0.067178	7642.12	0.005	0.056392	19114.57	0.002	0.041040	22356.55	0.001	0.034200
5001.31	0.02	0.089788	7971.60	0.01	0.065804	8435.47	0.005	0.054001	23031.47	0.002	0.036185	27568.22	0.001	0.033550
5455.99	0.02	0.085819	8674.04	0.01	0.064874	9303.42	0.005	0.053520	25929.57	0.002	0.036299	30005.22	0.001	0.032921
6737.99	0.02	0.081544	10711.81	0.01	0.063256	9827.46	0.005	0.052454	29205.40	0.002	0.036342	33654.20	0.001	0.032099
7469.47	0.02	0.080554	11649.57	0.01	0.058777	10504.40	0.005	0.052464	31887.66	0.002	0.034349	35899.69	0.001	0.031954
7952.33	0.02	0.079994	13933.31	0.01	0.056676	11028.45	0.005	0.052358	33598.52	0.002	0.035473	39554.21	0.001	0.032021
8576.20	0.02	0.079332	14636.36	0.01	0.055593	11729.29	0.005	0.051244	35847.58	0.002	0.033820	42667.88	0.001	0.031888
9200.89	0.02	0.078944	17082.10	0.01	0.054248	12449.70	0.005	0.050284	37476.60	0.002	0.034254	45770.10	0.001	0.031254
9593.68	0.02	0.078057	20223.45	0.01	0.051228	13810.12	0.005	0.047384	39644.52	0.002	0.033361	48663.11	0.001	0.031821
10239.14	0.02	0.077508	22856.28	0.01	0.050347	15692.88	0.005	0.046591	40163.65	0.002	0.033933	51204.00	0.001	0.030979
10804.97	0.02	0.077508	26901.11	0.01	0.049354	19134.91	0.005	0.044269	41432.69	0.002	0.032900	54324.45	0.001	0.031754
11495.09	0.02	0.077896	28283.28	0.01	0.048733	20036.20	0.005	0.043386	42793.35	0.002	0.034101	57441.20	0.001	0.031721
12347.80	0.02	0.076841	29421.40	0.01	0.048360	21063.20	0.005	0.043100	44500.52	0.002	0.033671	59822.10	0.001	0.030687
13916.97	0.02	0.075774	32621.09	0.01	0.047956	22364.41	0.005	0.042013	46170.63	0.002	0.032932			
14874.17	0.02	0.075695	36326.22	0.01	0.047284	24771.00	0.005	0.040761	47794.91	0.002	0.033540			
			40066.90	0.01	0.046078	26607.06	0.005	0.040381						
						28054.58	0.005	0.039947						
						30270.52	0.005	0.039015						
						32536.25	0.005	0.038573						
						35542.07	0.005	0.037272						
						37450.97	0.005	0.038374						
						40647.28	0.005	0.037409						
						42368.68	0.005	0.037221						
						44494.43	0.005	0.037970						
						47109.26	0.005	0.037058						

Table A-6: Experimental Data for Test Section 6 (Perforations, $\alpha = 90^{o}$, $\varphi = 5$ shots/ft)

N_{Re}	q_{in}/Q	f_T	N_{Re}	q_{in}/Q	f_T	N_{Re}	q_{in}/Q	f_T	N_{Re}	q_{in}/Q	f_T	N_{Re}	q_{in}/Q	f_T
4804.79	0.02	0.094491	8154.90	0.01	0.066729	9245.64	0.005	0.046871	18346.41	0.002	0.038120	24915.26	0.001	0.035649
5073.88	0.02	0.093624	9926.46	0.01	0.064780	11464.42	0.005	0.045039	22219.45	0.002	0.037093	29454.40	0.001	0.034726
5709.55	0.02	0.092555	11118.30	0.01	0.061504	13183.12	0.005	0.048407	25058.08	0.002	0.036798	30947.22	0.001	0.034453
8597.35	0.02	0.089691	12053.82	0.01	0.059448	15193.05	0.005	0.045172	28798.16	0.002	0.035283	33112.29	0.001	0.032781
9267.26	0.02	0.086905	13137.75	0.01	0.058893	16963.08	0.005	0.045220	31922.61	0.002	0.034518	34958.74	0.001	0.032043
9973.58	0.02	0.083899	14969.89	0.01	0.056433	18619.92	0.005	0.043402	33404.96	0.002	0.033957	39293.13	0.001	0.032704
12041.58	0.02	0.080373	15951.63	0.01	0.056507	20728.58	0.005	0.042346	35324.56	0.002	0.033383	42035.31	0.001	0.030874
11727.03	0.02	0.079372	17274.96	0.01	0.055400	22606.09	0.005	0.042008	37409.93	0.002	0.032553	44782.29	0.001	0.031815
12332.63	0.02	0.078815	18663.13	0.01	0.054100	24242.08	0.005	0.040169	39289.40	0.002	0.032325	47534.07	0.001	0.032297
13513.21	0.02	0.077145	19786.93	0.01	0.053200	26313.59	0.005	0.040777	42212.69	0.002	0.032217	50290.68	0.001	0.032448
13950.12	0.02	0.077627	21105.99	0.01	0.052800	28923.69	0.005	0.040100	46679.23	0.002	0.032323	53052.11	0.001	0.032360
14972.67	0.02	0.077242	24404.27	0.01	0.051218	30108.78	0.005	0.039990	50961.14	0.002	0.032110	55818.40	0.001	0.032098
15799.79	0.02	0.076599	29266.75	0.01	0.049925	32084.03	0.005	0.038775	55232.63	0.002	0.031519	58589.55	0.001	0.031710
18129.29	0.02	0.074430	31442.66	0.01	0.049017	34550.00	0.005	0.038038	59771.16	0.002	0.030352			
20555.00	0.02	0.072820	33560.07	0.01	0.048072	36777.00	0.005	0.037999	62175.81	0.002	0.031767			
22222.00	0.02	0.071220	39797.99	0.01	0.047074	38995.00	0.005	0.037956						
25136.00	0.02	0.071099	43699.75	0.01	0.047689	41354.58	0.005	0.037908						
27800.00	0.02	0.069550				42995.00	0.005	0.037871						
29776.78	0.02	0.069700												
32335.00	0.02	0.068540												
35002.00	0.02	0.069220												

Table A-7: Experimental Data for Test Section 7 (Perforations, $\alpha = 360^{o}$, $\varphi = 10$ shots/ft):

N_{Re}	q_{in}/Q	f_T	N_{Re}	q_{in}/Q	f_T	N_{Re}	q_{in}/Q	f_T	N_{Re}	q_{in}/Q	f_T	N_{Re}	q_{in}/Q	f_T
2490.44	0.02	0.208201	5002.84	0.01	0.131769	6866.27	0.005	0.085441	15790.60	0.002	0.053111	11456.74	0.001	0.049752
2912.00	0.02	0.193784	6855.09	0.01	0.124248	8727.37	0.005	0.078388	18800.86	0.002	0.051160	14924.77	0.001	0.043065
3449.70	0.02	0.186991	10831.24	0.01	0.109099	10218.46	0.005	0.070172	21292.99	0.002	0.050987	16490.85	0.001	0.042132
4466.99	0.02	0.181081	12360.20	0.01	0.105069	11233.41	0.005	0.070273	22092.45	0.002	0.050665	18056.93	0.001	0.041198
5395.19	0.02	0.181990	13272.56	0.01	0.104527	12006.51	0.005	0.069535	23726.32	0.002	0.046235	19972.58	0.001	0.040163
6436.03	0.02	0.179640	14664.47	0.01	0.109396	14073.93	0.005	0.069737	26248.23	0.002	0.044148	21888.23	0.001	0.039128
8294.21	0.02	0.170978	16835.98	0.01	0.105284	15476.22	0.005	0.066633	29632.05	0.002	0.043345	25711.39	0.001	0.037851
10829.31	0.02	0.169547	19132.18	0.01	0.107289	16838.70	0.005	0.065036	33666.23	0.002	0.044442	30070.78	0.001	0.037953
11803.46	0.02	0.169357	21965.10	0.01	0.102586	17978.24	0.005	0.064188	34814.51	0.002	0.041636	29534.55	0.001	0.036574
12787.70	0.02	0.167358	23743.55	0.01	0.103891	19518.90	0.005	0.061680	39038.48	0.002	0.041512	34430.17	0.001	0.038055
13782.17	0.02	0.167007	25924.43	0.01	0.101950	21767.28	0.005	0.060836	42608.12	0.002	0.041308	40061.67	0.001	0.036474
14787.01	0.02	0.166536	28852.24	0.01	0.102838	24133.10	0.005	0.062152	46217.43	0.002	0.040626	43728.33	0.001	0.037449
15802.37	0.02	0.166704	31457.58	0.01	0.102298	26864.85	0.005	0.061389	49573.87	0.002	0.040220	47404.69	0.001	0.037649
16828.39	0.02	0.164763	34113.84	0.01	0.100309	29613.56	0.005	0.061034	52488.35	0.002	0.040428	51090.80	0.001	0.037361
			38089.37	0.01	0.100730	32025.87	0.005	0.060480						
			41429.11	0.01	0.100354	33744.02	0.005	0.062683						
			45301.89	0.01	0.102333	36184.27	0.005	0.061399						
						38639.80	0.005	0.059892						
						40752.78	0.005	0.059423						

Table A-8: Experimental Data for Test Section 8 (Perforations, $\alpha = 90^{o}$, $\varphi = 10$ shots/ft)

N_{Re}	q_{in}/Q	f_T	N_{Re}	q_{in}/Q	f_T	N_{Re}	q_{in}/Q	f_T	N_{Re}	q_{in}/Q	f_T	N_{Re}	q_{in}/Q	f_T
1990.85	0.02	0.096000	6900.60	0.01	0.072473	15948.51	0.005	0.047882	18364.76	0.002	0.040120	24952.60	0.001	0.035512
2369.38	0.02	0.095699	8771.00	0.01	0.070504	18988.87	0.005	0.046789	22241.67	0.002	0.038994	29491.81	0.001	0.034613
2607.01	0.02	0.094932	10269.55	0.01	0.069377	21505.92	0.005	0.045815	25083.14	0.002	0.038701	30984.52	0.001	0.034347
3291.67	0.02	0.093934	11289.58	0.01	0.069048	22313.37	0.005	0.045500	28826.96	0.002	0.036519	33149.49	0.001	0.032686
3836.78	0.02	0.092176	12066.55	0.01	0.068751	23963.59	0.005	0.044159	31954.53	0.002	0.036443	34995.98	0.001	0.031955
4209.53	0.02	0.091516	14144.30	0.01	0.067957	26510.71	0.005	0.043117	33438.37	0.002	0.035870	39370.26	0.001	0.032540
4819.15	0.02	0.089404	15553.60	0.01	0.066885	29928.37	0.005	0.042333	35359.89	0.002	0.035299	42077.35	0.001	0.030794
5912.90	0.02	0.088385	16922.89	0.01	0.065306	34002.90	0.005	0.042412	37447.34	0.002	0.034443	44827.07	0.001	0.031733
6515.05	0.02	0.087457	18068.13	0.01	0.064674	35162.65	0.005	0.041661	39328.69	0.002	0.033242	47581.61	0.001	0.031215
7857.65	0.02	0.086100	19616.49	0.01	0.063986	39428.86	0.005	0.040541	42254.90	0.002	0.033214	50340.97	0.001	0.031237
8751.17	0.02	0.085434	21876.11	0.01	0.062153	43034.20	0.005	0.040342	46725.90	0.002	0.032941	53105.16	0.001	0.031228
10221.72	0.02	0.083955	24253.76	0.01	0.061457	46679.60	0.005	0.039673	51012.10	0.002	0.032628	55874.22	0.001	0.031202
11860.46	0.02	0.084296	26999.18	0.01	0.060702	50069.61	0.005	0.039275	55287.87	0.002	0.032438	58648.14	0.001	0.031029
14470.50	0.02	0.083318	29761.63	0.01	0.060352	53013.23	0.005	0.039478	59830.93	0.002	0.031274			
16330.99	0.02	0.082468	32186.00	0.01	0.059804				62237.98	0.002	0.031686			
			33912.74	0.01	0.061984									
			36365.19	0.01	0.060713									
			38833.00	0.01	0.059221									
			40956.55	0.01	0.058756									

Table A-9: Experimental Data for Test Section 9 (Perforations, $\alpha = 360^{o}$, $\varphi = 20$ shots/ft)

N_{Re}	q_{in}/Q	f_T	N_{Re}	q_{in}/Q	f_T	N_{Re}	q_{in}/Q	f_T	N_{Re}	q_{in}/Q	f_T	N_{Re}	q_{in}/Q	f_T
2266.12	0.02	0.255764	6102.74	0.01	0.149285	6522.96	0.005	0.095995	15853.77	0.002	0.052615	11456.74	0.001	0.049752
2630.74	0.02	0.252021	8844.41	0.01	0.141299	8291.00	0.005	0.088026	18876.06	0.002	0.049802	14924.77	0.001	0.043065
3127.15	0.02	0.249357	11678.93	0.01	0.136340	9369.43	0.005	0.085387	21350.50	0.002	0.050356	16500.66	0.001	0.042372
4055.51	0.02	0.242736	12678.79	0.01	0.134829	10212.15	0.005	0.087080	22104.73	0.002	0.050584	18080.71	0.001	0.041174
4904.47	0.02	0.239527	13403.56	0.01	0.132772	11065.67	0.005	0.083553	23004.88	0.002	0.049932	20010.81	0.001	0.040440
5865.55	0.02	0.234775	14780.61	0.01	0.131984	13370.23	0.005	0.078240	25140.06	0.002	0.048735	21946.00	0.001	0.039082
7503.81	0.02	0.232823	16532.68	0.01	0.128277	14676.61	0.005	0.077989	28124.57	0.002	0.048581	25810.84	0.001	0.039503
9794.93	0.02	0.223339	18291.96	0.01	0.127064	15408.27	0.005	0.079355	32142.32	0.002	0.048631	30204.53	0.001	0.041558
10661.17	0.02	0.221904	20429.39	0.01	0.129146	16524.17	0.005	0.077545	32688.43	0.002	0.047708	29691.03	0.001	0.036487
11534.01	0.02	0.219506	21460.69	0.01	0.129532	17498.83	0.005	0.078791	36300.13	0.002	0.048219	34612.79	0.001	0.037970
12413.51	0.02	0.218394	22742.42	0.01	0.129063	19282.43	0.005	0.079770	40007.99	0.002	0.045844	40263.76	0.001	0.036396
13299.75	0.02	0.213877	24529.17	0.01	0.128675	21735.75	0.005	0.078489	42000.13	0.002	0.047734	43949.17	0.001	0.037372
14192.78	0.02	0.212792	25871.97	0.01	0.128710	24202.27	0.005	0.077480	43997.97	0.002	0.047268	47644.38	0.001	0.037573
15092.68	0.02	0.212199	27084.60	0.01	0.127995	26370.95	0.005	0.079012	46001.55	0.002	0.047623	51349.43	0.001	0.037286
15999.52	0.02	0.211973				28303.65	0.005	0.079618	48010.88	0.002	0.048088			
16913.37	0.02	0.212637				30673.90	0.005	0.077492	50026.00	0.002	0.048458			
17834.31	0.02	0.211956				32596.53	0.005	0.077459						
18762.43	0.02	0.212941				34923.69	0.005	0.075050						
19697.79	0.02	0.211931				36209.50	0.005	0.077340						
22339.08	0.02	0.211958												

Table A-10: Experimental Data for Test Section 10 (Perforations, $\alpha = 180^{o}$, $\varphi = 20$ shots/ft)

N_{Re}	q_{in}/Q	f_T	N_{Re}	q_{in}/Q	f_T	N_{Re}	q_{in}/Q	f_T	N_{Re}	q_{in}/Q	f_T	N_{Re}	q_{in}/Q	f_T
2286.06	0.02	0.258600	7342.67	0.01	0.145500	8922.89	0.005	0.085080	16443.70	0.002	0.044214	17270.60	0.001	0.035222
2660.67	0.02	0.243300	9094.34	0.01	0.130080	9200.93	0.005	0.077180	19476.00	0.002	0.041815	18860.64	0.001	0.034254
3167.09	0.02	0.228900	11938.87	0.01	0.128950	9789.37	0.005	0.075613	21960.44	0.002	0.042245	21800.74	0.001	0.033672
4105.45	0.02	0.213595	12948.73	0.01	0.126550	10642.08	0.005	0.076384	22724.66	0.002	0.042400	23745.94	0.001	0.032568
4964.40	0.02	0.220800	13683.49	0.01	0.123550	11505.61	0.005	0.071911	23634.81	0.002	0.041819	26620.77	0.001	0.032947
5935.48	0.02	0.214330	15770.54	0.01	0.122370	13820.17	0.005	0.069637	25779.99	0.002	0.040782	28495.60	0.001	0.033325
7583.74	0.02	0.209823	16832.61	0.01	0.120180	15136.55	0.005	0.068451	28774.50	0.002	0.040619	30370.44	0.001	0.033100
9884.87	0.02	0.198850	18601.90	0.01	0.121590	15878.21	0.005	0.067893	32802.25	0.002	0.040628	31024.47	0.001	0.034690
10761.10	0.02	0.196750	20749.32	0.01	0.122500	17004.11	0.005	0.066135	33358.36	0.002	0.039823	33520.96	0.001	0.030482
11643.94	0.02	0.193450	22790.63	0.01	0.120298	17988.76	0.005	0.067459	36980.07	0.002	0.040216	35452.73	0.001	0.031748
12533.45	0.02	0.192250	23082.36	0.01	0.120080	19782.37	0.005	0.068516	40697.93	0.002	0.038204	37384.49	0.001	0.031112
13429.68	0.02	0.190020	24879.10	0.01	0.119980	22245.69	0.005	0.067287	42700.06	0.002	0.039745	40333.59	0.001	0.030444
14332.71	0.02	0.191150	26231.90	0.01	0.119750	24722.20	0.005	0.066331	44707.90	0.002	0.039324	42113.70	0.001	0.030457
15242.61	0.02	0.188750	27454.53	0.01	0.120036	26900.88	0.005	0.067951	46721.48	0.002	0.039587	44809.11	0.001	0.031300
16159.45	0.02	0.186630	29501.29	0.01	0.119888	28843.59	0.005	0.067633	48740.82	0.002	0.039940	46514.32	0.001	0.031494
17083.30	0.02	0.186750				31223.83	0.005	0.066939	50765.93	0.002	0.040214	51229.36	0.001	0.031280
18014.25	0.02	0.179950				33156.46	0.005	0.067572						
18952.36	0.02	0.180450				35493.62	0.005	0.064185						
19897.72	0.02	0.180010				36789.43	0.005	0.064581						
22549.01	0.02	0.182350												
25200.30	0.02	0.180690												
27851.59	0.02	0.183030												